

# CRC-Aided List Decoding of Convolutional Codes in the Short Blocklength Regime

Hengjie Yang, *Student Member, IEEE* Ethan Liang, *Student Member, IEEE* Minghao Pan,  
and Richard D. Wesel, *Fellow, IEEE*

**Abstract**—This paper identifies convolutional codes (CCs) used in conjunction with a CC-specific cyclic redundancy check (CRC) code as a promising paradigm for short blocklength codes. The resulting CRC-CC concatenated code naturally permits the use of the serial list Viterbi decoding (SLVD) to achieve maximum-likelihood decoding. The CC of interest is of rate- $1/\omega$  and is either zero-terminated (ZT) or tail-biting (TB). For CRC-CC concatenated code designs, we show how to find the optimal CRC polynomial for a given ZTCC or TBCC. Our complexity analysis reveals that SLVD decoding complexity is a function of the terminating list rank, which converges to one at high SNR. This behavior allows the performance gains of SLVD to be achieved with a small increase in average complexity at the SNR operating point of interest. With a sufficiently large CC constraint length, the performance of CRC-CC concatenated code under SLVD approaches the random-coding union (RCU) bound as the CRC size is increased while average decoding complexity does not increase significantly. TB encoding further reduces the backoff from the RCU bound by avoiding the termination overhead. As a result, several CRC-TBCC codes outperform the RCU bound at moderate SNR values while permitting decoding with relatively low complexity.

**Index Terms**—Convolutional code, cyclic redundancy check (CRC) code, list Viterbi decoding, negative acknowledgement (NACK), undetected errors.

## I. INTRODUCTION

RECENTLY, the coding theory community has witnessed a growing interest in designing powerful short blocklength codes (e.g., codes with a thousand or fewer information bits). This renewed interest is mainly driven by the stringent requirement of new ultra-reliable low-latency communication in 5G [4], and advances in the finite-blocklength information theory developed by Polyanskiy, Poor and Verdú [5]. The basic question of finite-blocklength information theory asks: what is the maximal channel coding rate achievable at a given blocklength  $n$  and error probability  $\epsilon$ ? To answer this question,

Polyanskiy *et al.* developed the *random coding union (RCU) bound*  $\text{rcu}(n, M)$  [5, Thm. 16] and the *meta-converse (MC) bound*  $\text{mc}(n, M)$  [5, Thm. 27] that provide, respectively, tight upper and lower bounds on the error probability  $P_e^*(n, M)$  of the best  $(n, M)$  code of length  $n$  and  $M$  codewords. Namely,

$$\text{mc}(n, M) \leq P_e^*(n, M) \leq \text{rcu}(n, M). \quad (1)$$

They also provide the *normal approximation (NA)* [5, Eq. 223] that tightly approximates the performance of the best  $(n, M)$  code. Thereafter, these bounds serve as benchmarks to assess the goodness of a given finite-blocklength code over a broad class of channels, including the discrete memoryless channel (DMC) and the additive white Gaussian noise (AWGN) channel. However, an accurate computation of the RCU and MC bounds involves integrating the tail probability of  $n$ -dimensional random variables, which becomes hard even for simple channels and moderate blocklengths. This motivates saddlepoint approximations of these bounds that only involve integrals of one-dimensional random variables [6].

For coding theorists, a central task is to construct *structured* short-blocklength codes for the binary AWGN channel such that the probability of error can fall into the region delimited by the RCU bound and the MC bound at a reasonable decoding complexity. There are numerous approaches to achieve this goal. As a comprehensive overview, Coşkun *et al.* surveyed in detail the contemporary short-blocklength code design developed in recent decades [7]. Important examples include ordered statistics decoding of classical block codes [8], [9] tail-biting convolutional codes [10], low-density parity-check codes [11], [12], turbo codes [13] and polar codes [14], [15]. Recent advances also include the polarization-adjusted CCs proposed by Arıkan [16], [17]. It is worth noting that if no restrictions are imposed on what kind of codes should be used for the AWGN channel, Shannon [18] has ingeniously shown that the optimal  $(n, M)$  code should be placed on a sphere in the  $n$ -dimensional Euclidean space such that the total solid angle are evenly split between the  $M$  Voronoi regions and every Voronoi region is a perfect circular cone in order to achieve the minimum probability of error.

While there are many possible structures for short-blocklength coding, this paper focuses on the concatenation of a convolutional code (CC) with a cyclic redundancy check (CRC) code. CCs were first introduced by Elias [19]. Viterbi decoding of CCs was developed by Viterbi [20] and its maximum-likelihood (ML) nature was recognized by Forney [21], [22]. The term “CRC” stems from the use of cyclic codes for error detection [23], where the cyclic codeword can be put

This paper was presented in part at IEEE GLOBECOM 2018, 2019 [1], [2] and IEEE ISIT 2020 [3].

This research is supported in part by National Science Foundation (NSF) grant CCF-2008918 and a Qualcomm Faculty Award. Any opinions, findings, and conclusions or recommendations expressed in this material are those of the author(s) and do not necessarily reflect the views of the NSF or of Qualcomm.

H. Yang is with the Department of Electrical and Computer Engineering, University of California, Los Angeles, Los Angeles, CA, 90095 USA (e-mail: hengjie.yang@ucla.edu).

E. Liang is with the Department of Electrical Engineering, Stanford University, Stanford, CA, 94305 USA (e-mail: emliang@stanford.edu)

M. Pan is with the Department of Mathematics, University of California, Los Angeles, Los Angeles, CA, 90095 USA (e-mail: minghaoan@ucla.edu).

R. D. Wesel is with the Department of Electrical and Computer Engineering, University of California, Los Angeles, Los Angeles, CA, 90095 USA (e-mail: wesel@ucla.edu).

into systematic form with the parity bits easily generated by a linear sequential circuit. In this paper as in many practical error detection applications, a linear sequential circuit is used to compute the parity bits, but the code is not required to be cyclic. The term “CRC” is retained nonetheless.

The structure of concatenating a CC with a CRC code was first proposed in the context of hybrid automatic repeat request (ARQ) [24] and is used in numerous practical systems where the CC serves as an inner error-correcting code to combat channel errors and the CRC code serves as an error-detecting code to verify if a codeword has been correctly received. Examples include the 3GPP cellular communications standard [25].

The classical decoding approach for a concatenated CRC-CC in a hybrid ARQ setting is Viterbi decoding with CRC verification. The codeword identified by Viterbi decoding is checked to determine whether it is divisible by the CRC polynomial. This indicates whether a valid message has been decoded. If the decoded sequence is divisible by the CRC polynomial, the message segment of the decoded sequence is declared as the most likely message. Otherwise, a negative acknowledgement (NACK) is declared and perhaps a retransmission request is sent to the transmitter.

Unfortunately, the classical approach of Viterbi decoding with CRC verification conceals the true potential of the CRC-CC concatenated codes. Performing a single Viterbi decoding step causes the decoder to give up too early, often before encountering a convolutional codeword that passes the CRC verification. To unleash the power of the CRC-CC concatenated code, we consider serial list Viterbi decoding (SLVD), which was pioneered by Seshadri and Sundberg [26]. SLVD sequentially performs multiple Viterbi decoding attempts, producing a rank ordered list of the convolutional codewords according to their likelihood. Hence, CRC verification can naturally be used as a termination criterion for this list decoding.

The SLVD terminates either when an input sequence passes the CRC verification or when the list rank reaches a specified maximum. We refer to this final list rank as the *terminating list rank*  $L$ . Note that  $L$  is a random variable that could be different for different noise realizations. As we will see, the decoding complexity for a particular noise realization increases with  $L$ , and the average complexity is a function of average list rank  $E[L]$ . The size of the convolutional codebook is a trivial but loose upper bound on the maximum value of  $L$ .

To constrain the peak decoding complexity, a *constrained maximum list size*  $\Psi$  can limit the largest possible terminating list rank. Constraining  $L \leq \Psi$  produces three possible outcomes: 1) a correct decoding if SLVD indeed identifies the transmitted message within  $\Psi$  trials; 2) an *undetected error* (UE) if an erroneous input is the first sequence found by SLVD that passes the CRC verification; and 3) a NACK and the forced termination of decoder if the SLVD fails to find an input sequence that passes CRC verification within  $\Psi$  trials. Note that there is a *supremum list rank*  $\lambda$  which is the maximum possible value of the terminating list rank  $L$ . Any value of  $\Psi \geq \lambda$  gives the same decoder behavior where the decoder does not produce any NACK. In the extreme case where  $\Psi = 1$ , the SLVD reduces to the classical Viterbi

decoding with CRC verification. If  $\Psi \geq \lambda$ , no NACK occurs and SLVD is an implementation of ML decoding of the CRC-CC concatenated code.

This paper focuses on the concatenation of a rate- $1/\omega$  CC with an optimized CRC code. We explore both zero-terminated (ZT) and tail-biting (TB) [27] CCs. To avoid ambiguity, the concatenated code is called a *CRC-ZTCC code* in the first case and a *CRC-TBCC code* in the second case. For CRC-ZTCC codes, Lou *et al.* [28] realized that previous designs of CRC polynomials typically ignore the structure of the inner error-correcting code, which leads to sub-optimal performance. Lou *et al.* designed optimal CRC polynomials for a given ZTCC such that the probability of UE is minimized for a single Viterbi decoding attempt followed by CRC verification. A key point in their analysis is that when the target probability of UE is low enough, the design principle is equivalent to maximizing the minimum distance of the CRC-ZTCC code. However, Lou *et al.* did not address the optimal CRC design for a TBCC and did not consider SLVD.

Compared to the CRC-ZTCC code, CRC-TBCC code has the advantage of avoiding the rate loss incurred by the overhead associated with the zero tail that follows the information sequence, but this overhead reduction comes with an increase in decoding complexity. A TB codeword requires that the initial and terminating states be the same, which can be achieved, for example, by setting the initial encoder memory to be the final bits of the information sequence. However, this requirement increases the difficulty of efficiently identifying the ML path on the trellis because the common value of the initial and terminating states is unknown at the decoder.

One approach to ML decoding of a TBCC is to perform Viterbi decoding from every possible initial state [27]. Various *approximate* algorithms are proposed for decoding the TBCC based on either the ML or maximum a posteriori (MAP) criteria, e.g., [29]–[32]. Among these algorithms, the wrap-around Viterbi algorithm (WAVA) [32] proves to be both efficient and near-ML. Shankar *et al.* [33] introduced an efficient, iterative, two-phase algorithm for *exact* ML decoding of TBCC, where an A\* algorithm is applied in the second phase, using information from the first phase to compute the heuristic function. To make the exact SLVD of TBCC possible and efficient, this paper extends Shankar *et al.*’s algorithm to accommodate the CRC polynomial. Specifically, if a traceback identifies a TB path, the CRC of the corresponding input sequence is checked. If the input sequence passes the CRC verification, the algorithm terminates. Otherwise, the algorithm locates the next rank ordered path.

### A. Contributions

This paper provides a design paradigm for both CRC-ZTCC codes and CRC-TBCC codes, a suite of tools for performance analysis of these codes, and a complexity analysis showing that SLVD allows low-complexity decoding at the desired operating point of probability of UE for  $\Psi \geq \lambda$ , i.e., a decoding complexity similar to standard Viterbi decoding of the CC alone. These contributions combine to yield, for example, CRC-CC concatenated codes that closely approach

the RCU bound while requiring decoding complexity similar to Viterbi decoding on a convolutional code trellis with  $2^8$  states.

1) *CRC-CC Design*: This paper introduces the concept of the *distance-spectrum optimal (DSO) CRC polynomial*, which minimizes the theoretical union bound of the probability of UE for  $\Psi \geq \lambda$ . Theorem 1 shows that for high SNR, the DSO CRC polynomial reduces to the one that obtains the best minimum distance  $d_{\min}^l$ . Theorem 2 provides a sharp upper bound on the achievable  $d_{\min}^l$  based on the distance spectrum of the CC. We present an efficient algorithm for finding DSO CRC polynomials for TBCCs of arbitrary rate, and provide DSO CRC polynomials for rate-1/2 ZT and TB CCs with a range of encoder complexities for 64 message bits.

2) *CRC-CC Performance Analysis*: The performance of a CRC-CC concatenated code with the constrained maximum list size  $\Psi$  is measured by three probabilities: probability of correct decoding  $P_{c,\Psi}$ , probability of UE  $P_{e,\Psi}$  and probability of NACK  $P_{NACK,\Psi}$ , where  $P_{c,\Psi} + P_{e,\Psi} + P_{NACK,\Psi} = 1$ . This paper provides bounds, approximations, and simulation results characterizing how these probabilities vary with  $\Psi$  and with SNR. Theorems 4 – 6 describe how performance evolves as  $\Psi$  increases, the existence and behavior of the supremum list rank  $\lambda$ , and performance (in terms of  $P_{c,\Psi}$ ,  $P_{e,\Psi}$ , and  $P_{NACK,\Psi}$ ) as a function of SNR for extreme values of  $\Psi = 1$  and  $\Psi = \lambda$ .

3) *CRC-CC Decoding Complexity*: This paper provides expressions of the complexity of SLVD for CRC-ZTCC codes and CRC-TBCC codes. These expressions reveal that complexity is a function of the expected list rank  $E[L]$ . This paper characterizes  $E[L]$  including a new approach to computing  $E[L]$  in the limit of low SNR, and a new analysis of conditional expected list rank given the noise magnitude, and two new approaches for approximating the conditional expected list rank. These approximations of conditional expected list rank naturally lead to an accurate approximation of  $E[L]$  as a function of  $P_{e,\lambda}$  which shows that as  $P_{e,\lambda}$  converges to 0,  $E[L]$  converges to 1. We see that for practically interesting operating points of  $P_{e,\lambda}$  such as  $10^{-6}$ ,  $E[L] \approx 1$  for typical CRC lengths. This implies that for an interesting range of CRC lengths, the CRC length can be increased with negligible impact on complexity. Moreover, for these CRC lengths, the complexity of SLVD for the CRC-CC concatenated code is very similar to that of standard Viterbi decoding of the CC alone.

4) *Achieving the RCU Bound with Practical Complexity*: Simulation results compared with the RCU bound show that for  $\nu = 8$  memory elements, our CRC-ZTCC designs can approach the RCU bound within 0.4 dB with decoding complexity similar to standard Viterbi decoding of the ZTCC. Our  $\nu = 8$  CRC-TBCC designs essentially achieve the RCU bound, but require increased decoding complexity.

## B. Organization

This paper is organized as follows: Sec. II reviews notation, the architecture of the CRC-aided list decoding of CCs, TB trellises, Polyanskiy *et al.*'s finite-blocklength bounds, and the related saddlepoint approximations. Sec. III introduces the

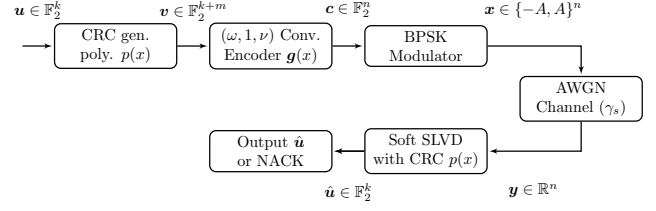


Fig. 1. Block diagram of the CRC-aided list decoding of CCs.

concept of the DSO CRC polynomial, shows that at high SNR the DSO CRC can be obtained by maximizing  $d_{\min}^l$ , provides an upper bound on  $d_{\min}^l$ , and gives a DSO CRC design algorithm for TBCCs of arbitrary rate at high SNR. Sec. IV presents the performance and complexity analyses of SLVD of a given CRC-CC concatenated code. Sec. V presents simulation results of our designed CRC-CC concatenated code. Sec. VI concludes the paper.

## II. PRELIMINARIES

### A. Notation

Let  $\mathbb{F}_2 = \{0, 1\}$  denote the binary field.  $\mathbb{F}_2^n$  denotes the set of  $n$ -dimensional binary sequences.  $\mathbb{F}_2[x]$  denotes the set of binary polynomials. The indicator function  $\mathbf{1}_E$  takes the value 1 if the event  $E$  occurs, and 0 otherwise. The polynomial  $u(x) = \sum_{i=0}^{n-1} u_i x^i \in \mathbb{F}_2[x]$  and its row vector form  $\mathbf{u} = [u_0, u_1, \dots, u_{n-1}] \in \mathbb{F}_2^n$  are used interchangeably. The CRC polynomial is represented in hexadecimal when its binary version is written from highest order to lowest order. For instance, 0xD represents  $x^3 + x^2 + 1$ . The convolutional generator polynomial is represented in octal when its binary version is written from lowest order to highest order. For instance, (13, 17) represents  $(1+x^2+x^3, 1+x+x^2+x^3)$ .  $E[\cdot]$  and  $P(\cdot)$  denote the expectation and the probability of an event over the underlying probability space, respectively.  $w_H(\cdot)$ ,  $d_H(\cdot, \cdot)$  and  $\|\cdot\|$  denote the Hamming weight, Hamming distance, and Euclidean norm respectively.  $\text{cl}(S)$ ,  $\partial(S)$  denotes the closure and the boundary of a subset  $S \subseteq \mathbb{R}^n$ , respectively.

### B. Architecture of CRC-Aided List Decoding of CCs

This paper considers CRC-aided list decoding of CCs, as depicted in Fig. 1. Let  $u(x) = \sum_{i=0}^{k-1} u_i x^i \in \mathbb{F}_2[x]$  denote the  $k$ -bit binary information sequence, where  $u_{k-1}$  is the first bit entering the CRC encoder. The information sequence  $u(x)$  is first pre-encoded with a degree- $m$  CRC generator polynomial  $p(x) = \sum_{i=0}^m p_i x^i \in \mathbb{F}_2[x]$  to obtain  $m$  parity check bits  $r(x) = x^m u(x) \bmod p(x)$ . Thus, we obtain  $v^*(x) = x^m u(x) + r(x)$  which is divisible by the CRC polynomial  $p(x)$ . The final CRC-coded sequence  $v(x)$  is produced by reversing  $v^*(x)$ , i.e.,  $v(x) = x^{k+m-1} v^*(x^{-1})$ . This guarantees that the first bit entering the encoder, namely,  $u_{k-1}$  in  $u(x)$ , is always the lowest degree term of  $v(x)$ , consistent with common representation. The CRC-coded sequence  $v(x)$  is then convolutionally encoded with a minimal, feed-forward,  $(\omega, 1, \nu)$  encoder  $\mathbf{g}(x) = [g_1(x), g_2(x), \dots, g_\omega(x)]$ ,  $g_i(x) = \sum_{j=0}^{\nu} g_{i,j} x^j$ , with  $\nu$  memory elements. In this paper, we do not require the CRC to be a cyclic code. Hence,  $p(x)$

only needs to satisfy  $p_0 = p_m = 1$ . The convolutional encoder  $g(x)$  is either ZT or TB.

This paper focuses on CRC-CC concatenated codes, but our analysis also involves the higher-rate CC for which the CRC codeword  $v$  is the input message. To describe the two codes of interest as concisely as possible, define the higher-rate code  $C_h$  and the lower-rate code  $C_l$ , which is also the CRC-CC concatenated code, as follows.

$$C_h \triangleq \{c \in \mathbb{F}_2^n : c = vG, \forall v \in \mathbb{F}_2^{k+m}\}. \quad (2)$$

$$C_l \triangleq \{c \in \mathbb{F}_2^n : c = vG, \forall v \in \mathbb{F}_2^{k+m} \text{ s.t. } p(x)|v^*(x)\}, \quad (3)$$

where  $G \in \mathbb{F}_2^{(k+m) \times n}$  is the matrix representation of the convolutional encoder. Intuitively, the effect of  $p(x)$  is to obtain a subcode  $C_l$  from the given higher-rate code  $C_h$ . The exact definition of  $C_h$  and  $C_l$  require the specification of the ZTCC or TBCC. For a ZTCC,  $n = \omega(k + m + \nu)$  and

$$G = \begin{bmatrix} G_0 & G_1 & \cdots & G_\nu \\ & G_0 & G_1 & \cdots & G_\nu \\ & & \ddots & \ddots & \ddots & \ddots \\ & & & G_0 & G_1 & \cdots & G_\nu \end{bmatrix},$$

where

$$G_i = [g_{1,i} \ g_{2,i} \ \cdots \ g_{\omega,i}], \quad i = 1, 2, \dots, \nu.$$

Similarly, for a TBCC,  $n = \omega(k + m)$  and

$$G = \begin{bmatrix} G_0 & G_1 & \cdots & \cdots & G_\nu \\ & G_0 & G_1 & \cdots & \cdots & G_\nu \\ & & \ddots & \ddots & \ddots & \ddots \\ & & & G_0 & G_1 & \cdots & \cdots & G_\nu \\ G_\nu & & & G_0 & G_1 & \cdots & G_{\nu-1} \\ G_{\nu-1} & G_\nu & & & \ddots & \ddots & \vdots \\ \vdots & & \ddots & & & \ddots & G_1 \\ G_1 & G_2 & \cdots & G_\nu & & & G_0 \end{bmatrix}.$$

Clearly,  $C_l \subseteq C_h$ ,  $|C_h| = 2^{k+m}$  and  $|C_l| = 2^k$ . The channel coding rate  $R = k/n$ . A fundamental quantity associated with a linear block code is its minimum distance. To aid our discussion, we define

$$d_{\min}^h \triangleq \min\{w_H(c) : c \in C_h \setminus \{0\}\} \quad (4)$$

$$d_{\min}^l \triangleq \min\{w_H(c) : c \in C_l \setminus \{0\}\}. \quad (5)$$

As a corollary,  $0 < d_{\min}^h \leq d_{\min}^l$ . Note that  $d_{\min}^l$  is equal to the free distance of the CC when a ZTCC is considered. However for TBCC,  $d_{\min}^l$  could be less than the free distance of the CC.

The binary phase shift keying (BPSK) modulated sequence  $\mathbf{x} = [x_0, x_1, \dots, x_{n-1}]$  is obtained via  $x_i = A(-1)^{c_i}$ , where  $A$  is the BPSK amplitude, and is then transmitted over the AWGN channel with channel SNR  $\gamma_s$ . Therefore, the channel model is

$$y_i = x_i + z_i, \quad i = 0, 1, \dots, n-1, \quad (6)$$

where  $z_i$ 's are independently and identically distributed (i.i.d.) according to the standard normal distribution  $\mathcal{N}(0, 1)$ . Thus  $\gamma_s = A^2$  or  $A = \sqrt{\gamma_s}$ .

Upon receiving the channel observations  $\mathbf{y}$ , the (soft) SLVD using CRC polynomial  $p(x)$  is employed to determine the most likely information sequences  $\hat{u}(x)$  from the trellis of the higher-rate code  $C_h$  based on  $\mathbf{y}$  in a sequential manner using a maximum of  $\Psi$  trials,  $1 \leq \Psi \leq |C_h|$ . The SLVD considered in this paper assumes that the sequentially produced rank ordered list of codewords<sup>1</sup> are automatically higher-rate codewords in  $C_h$ . Hence, decoding terminates and the list stops growing when the input sequence  $\hat{v}^*(x)$  of a higher-rate codeword passes the CRC verification. The corresponding list rank is marked as the terminating list rank  $L$  and the most likely information sequence  $\hat{u}(x)$  can be recovered from the last  $k$  bits of  $\hat{v}^*(x)$ . If an input sequence divisible by  $p(x)$  is not found after  $\Psi$  attempts, the decoder terminates at list rank  $\Psi$  with a NACK as the output. As introduced earlier, there exists a supremum list rank  $\lambda$  (whose formal definition will be given in (43)) which is solely determined by  $C_h$  and  $C_l$ . If  $\Psi \geq \lambda$ , no NACK will occur.

A UE occurs if the SLVD erroneously identifies an input sequence  $\hat{v}^*(x)$  that is divisible by  $p(x)$  and  $\hat{v}^*(x) \neq v^*(x)$ . This is equivalent to the case where the UE polynomial  $\hat{v}^*(x) - v^*(x) \in \mathbb{F}_2[x]$  is nonzero and is divisible by  $p(x)$ . Hence, an *error event* is given by the input-output pair  $(\hat{v}(x) - v(x), \hat{c}(x) - c(x))$  where  $\hat{v}(x) \neq v(x)$  and  $\hat{c}(x)$  is a higher-rate codeword. By linearity, the set of error events is the nonzero CRC-CC concatenated code. When restricted to CCs, we can also use a trellis path to represent an error event.

The performance of the CRC-CC concatenated code is thus measured by three probabilities: probability of correct decoding  $P_{c,\Psi}$ , probability of UE  $P_{e,\Psi}$  and probability of NACK  $P_{NACK,\Psi}$ , where  $P_{c,\Psi} + P_{e,\Psi} + P_{NACK,\Psi} = 1$ . In the special case where  $\Psi \geq \lambda$ ,  $P_{c,\Psi} + P_{e,\Psi} = 1$ . For ease of reference, we use  $P_{e,\lambda}$  to represent  $P_{e,\Psi}$  for which  $\Psi \geq \lambda$ .

### C. Tail-Biting Trellises

We follow [34] in describing the tail-biting trellises. Let  $V$  be a set of vertices (or states). The set  $\mathcal{A}$  is the output alphabet, and  $E$  is the set of edges described as ordered triples  $(v, a, v')$  with  $v, v' \in V$ , and  $a \in \mathcal{A}$ . In words,  $(v, a, v') \in E$  denotes an edge that starts at  $v$ , ends at  $v'$  and has output  $a$ .

**Definition 1** (Tail-biting trellises). *A tail-biting trellis  $T = (V, E, \mathcal{A})$  of depth  $N$  is an edge-labeled directed graph with the following property: the vertex set  $V$  can be partitioned as*

$$V = V_0 \cup V_1 \cup \cdots \cup V_{N-1} \quad (7)$$

*such that every edge in  $T$  either begins at a vertex of  $V_i$  and ends at a vertex of  $V_{i+1}$  for some  $i = 0, 1, \dots, N-2$ , or begins at a vertex of  $V_{N-1}$  and ends at a vertex of  $V_0$ .*

Geometrically, a TB trellis can be viewed as a cylinder of  $N$  sections defined on some circular time axis. Alternatively, we can also define a TB trellis on a sequential time axis  $\mathcal{I} = \{0, 1, \dots, N\}$  with the restriction that  $V_0 = V_N$  so that we obtain a conventional trellis.

<sup>1</sup>The input sequence that generates this higher-rate codeword is also known simultaneously.

For a trellis  $T$  of depth  $N$ , a trellis section connecting time  $i$  and  $i+1$  is a subset  $T_i \subseteq V_i \times \mathcal{A} \times V_{i+1} \subseteq E$  that specifies the allowed combination  $(s_i, a_i, s_{i+1})$  of state  $s_i \in V_i$ , output symbol  $a_i \in \mathcal{A}$ , and state  $s_{i+1} \in V_{i+1}$ ,  $i = 0, 1, \dots, N-1$ . Such allowed combinations are called trellis branches. A trellis path  $(\mathbf{s}, \mathbf{a}) \in T$  is a state/output sequence pair, where  $\mathbf{s} \in V_0 \times V_1 \times \dots \times V_N$ ,  $\mathbf{a} \in \mathcal{A}^N$ . Since  $\mathbf{s}$  equivalently specifies the input sequence, a trellis path  $(\mathbf{s}, \mathbf{a})$  is also an error event. The code represented by trellis  $T$  is the set of all output sequences  $\mathbf{a}$  corresponding to all trellis paths  $(\mathbf{s}, \mathbf{a})$  in  $T$ .

For a TB trellis  $T$  of depth  $N$ , a TB path  $(\mathbf{s}, \mathbf{a})$  of length  $N$  on  $T$  is a *closed* path through  $N$  vertices. If  $T$  is defined on a sequential time axis  $\mathcal{I} = \{0, 1, \dots, N\}$ , then any TB path  $(\mathbf{s}, \mathbf{a})$  of length  $N$  satisfies  $s_0 = s_N$ .

### D. Finite-Blocklength Bounds and Approximations

In [5], Polyanskiy *et al.* derived the RCU bound and the MC bound that upper and lower bound the probability of codeword error of the best  $(n, M)$  code. These two bounds serve as benchmarks to assess the performance of a given finite-blocklength code.

We follow the notation in [6] to introduce the RCU bound and the MC bound. Let  $W^n(\cdot|\cdot)$  denote a length- $n$  channel. Let  $\alpha_\beta(P, Q)$  denote the smallest type-I error probability among all tests discriminating between distributions  $P$  and  $Q$ , with a type-II error probability at most  $\beta$  [35, Ch. 11.7]. For a random-coding ensemble defined over distribution  $P^n$ , the RCU bound is given by

$$\text{rcu}(n, M) \triangleq \mathbb{E}[\min\{1, (M-1) \text{pep}(X^n, Y^n)\}], \quad (8)$$

where  $(X^n, Y^n) \sim P^n \times W^n$  and the pairwise error probability  $\text{pep}(x^n, y^n)$  is defined as

$$\text{pep}(x^n, y^n) \triangleq \mathbb{P}(W^n(y^n|\bar{X}^n) \geq W^n(y^n|x^n)),$$

with  $\bar{X}^n \sim P^n$ . The MC bound is a minimax of a particular smallest type-I error error probability

$$\text{mc}(n, M) \triangleq \min_{P^n} \max_{Q^n} \left\{ \alpha_{\frac{1}{M}}(P^n \times W^n, P^n \times Q^n) \right\}, \quad (9)$$

where the minimization is over all input distributions  $P^n$ , and the maximization is over a set of auxiliary, independent of the input, output distributions  $Q^n$ .

An exact evaluation of the RCU bound and the MC bound involves integrating tail probabilities of  $n$ -dimensional random variables, which is computationally difficult even for simple channels and moderate values of  $n$ . In [6], the authors provided saddlepoint approximations of these two bounds for memoryless symmetric channels, including the binary-input AWGN channel. These approximations are shown to be tight for a wide range of rates and blocklengths. Sec. V uses these saddlepoint approximations to evaluate the RCU bound and the MC bound.

**Approximation 1** (MC bound, [6]). *For memoryless symmetric channels for which  $Y \sim W(\cdot|x)$  is independent of  $x$ ,*

$$\text{mc}(n, M) \approx \max_{\rho \geq 0} \left\{ e^{-n(E_0(\rho) - \rho E'_0(\rho))} \left( \Psi(\sqrt{nU(\rho)}) + \Psi(\rho\sqrt{nU(\rho)}) - e^{-n(R - E'_0(\rho))} \right) \right\}, \quad (10)$$

where

$$E_0(\rho, P) = -\log \int_{\mathcal{Y}} \left( \sum_{x \in \mathcal{X}} P(x) W(y|x)^{\frac{1}{1+\rho}} \right)^{1+\rho} dy \quad (11)$$

$$E_0(\rho) = \max_P E_0(\rho, P) \quad (12)$$

$$\Psi(x) = \frac{1}{2} \text{erfc} \left( \frac{|x|}{\sqrt{2}} \right) e^{\frac{x^2}{2}} \text{sign}(x) \quad (13)$$

$$U(\rho) = -(1+\rho)E'_0(\rho), \quad (14)$$

where  $\mathcal{X}$  and  $\mathcal{Y}$  denote the input and output alphabets of the channel, and the maximization in (12) is over all possible probability distributions on  $\mathcal{X}$ .

**Approximation 2** (RCU bound, [6]). *For memoryless symmetric channels for which  $Y \sim W(\cdot|x)$  is independent of  $x$ ,*

$$\text{rcu}(n, M) \approx \tilde{\xi}_n(\hat{\rho}) + \psi_n(\hat{\rho}) e^{-n(E_0(\hat{\rho}, P) - \hat{\rho}R)}, \quad (15)$$

where  $\hat{\rho}$  is the value for which  $E'_0(\rho, P) = R$ , and

$$Q_\rho(y) = \frac{1}{e^{-E_0(\rho, P)}} \left( \sum_{x \in \mathcal{X}} P(x) W(y|x)^{\frac{1}{1+\rho}} \right)^{1+\rho} \quad (16)$$

$$\bar{\omega}''(\hat{\rho}) = \int_{\mathcal{Y}} Q_{\hat{\rho}}(y) \left[ \frac{\partial^2}{\partial \tau^2} \left( \log \sum_{x \in \mathcal{X}} P(x) W(y|x)^\tau \right) \right]_{\tau=\hat{\rho}} dy \quad (17)$$

$$\theta_n(\hat{\rho}) = \frac{1}{\sqrt{1+\hat{\rho}}} \left( \frac{1+\hat{\rho}}{\sqrt{2\pi n \bar{\omega}''(\hat{\rho})}} \right)^{\hat{\rho}} \quad (18)$$

$$\tilde{\xi}_n(\hat{\rho}) = \begin{cases} 1, & \hat{\rho} < 0 \\ 0, & 0 \leq \hat{\rho} \leq 1 \\ e^{-n(E_0(1, P) - R)} \theta_n(1), & \hat{\rho} > 1 \end{cases} \quad (19)$$

$$\psi_n(\hat{\rho}) = \theta_n(\hat{\rho}) \left( \Psi(\hat{\rho}\sqrt{nU(\rho)}) + \Psi((1-\hat{\rho})\sqrt{nU(\rho)}) \right). \quad (20)$$

### III. THE SEARCH OF THE DSO CRC POLYNOMIAL

In this section, we seek to design CRC-CC concatenated codes that provide the lowest possible probability of UE  $P_{e, \Psi}$ , where  $\Psi \geq \lambda$ . To this end, for a given CC, we design CRC polynomials that minimize the union bound on the probability of undetected error  $P_{e, \lambda}$ . The resulting CRC polynomial is known as the DSO CRC polynomial.

#### A. General Theory

For a given CC and a desired CRC degree  $m$ , we wish to identify the degree- $m$  CRC polynomial

$$p(x) = 1 + p_1x + \dots + p_{m-1}x^{m-1} + x^m \in \mathbb{F}_2[x] \quad (21)$$

that minimizes the probability of UE  $P_{e, \lambda}$ . Since the exact probability  $P_{e, \lambda}$  has no closed-form expression that can facilitate a design procedure, we use the union bound as an objective function that only involves the *distance spectrum*,  $C_{d_{\min}^l}, \dots, C_n$ , of the lower-rate code  $\mathcal{C}_l$ , where  $C_d$  is the number of codewords in  $\mathcal{C}_l$  of Hamming weight  $d$ ,  $d_{\min}^l \leq d \leq n$ . The distance spectrum of the lower-rate code is a function of both the CRC polynomial and the higher-rate code. For any

candidate polynomial  $p(x)$ , the union bound on  $P_{e,\lambda}$  is given by

$$\begin{aligned} P_{e,\lambda} &\leq \sum_{\mathbf{c} \in \mathcal{C}_l \setminus \{\bar{\mathbf{c}}\}} \mathbb{P}\left(Z > \frac{1}{2} \|\mathbf{x}(\mathbf{c}) - \mathbf{x}(\bar{\mathbf{c}})\| \mid \mathbf{X} = \mathbf{x}(\bar{\mathbf{c}})\right) \\ &= \sum_{d=d_{\min}^l}^n C_d Q(A\sqrt{d}), \end{aligned} \quad (22)$$

where  $\bar{\mathbf{c}} \in \mathcal{C}_l$  is the transmitted codeword,  $\mathbf{x}(\mathbf{c}) \in \{-A, A\}^n$  is the BPSK-modulated point for codeword  $\mathbf{c}$ ,  $Z \sim \mathcal{N}(0, 1)$ , and

$$Q(x) \triangleq \int_x^\infty \frac{1}{\sqrt{2\pi}} e^{-u^2/2} du \quad (23)$$

is the complementary Gaussian cumulative distribution function.  $Q(A\sqrt{d})$  computes the pairwise error probability of two codewords with distance  $d$ . For a given CC, a given SNR  $\gamma_s$  (i.e.,  $A = \sqrt{\gamma_s}$ ), and an objective CRC degree  $m$ , we define the degree- $m$  DSO CRC polynomial as the one that minimizes the union bound on  $P_{e,\lambda}$ . Namely, the degree- $m$  DSO CRC polynomial is the solution to the following optimization problem:

$$\min_{p(x)} \sum_{d=d_{\min}^l}^n C_d Q(A\sqrt{d}). \quad (24)$$

Theoretically, the distance spectrum  $C_{d_{\min}^l}, \dots, C_n$  of  $\mathcal{C}_l$  can be found through Viterbi search of the trellis of the higher-rate code  $\mathcal{C}_h$ , retaining only codewords whose input sequences are divisible by the candidate CRC polynomial  $p(x)$ . However, this approach requires the calculation of distance spectra for  $2^{m-1}$  candidate CRC polynomials and quickly becomes computationally expensive as  $k$  gets large. The degree- $m$  DSO CRC polynomial depends on the specific higher-rate code and the SNR at which  $P_{e,\lambda}$  is being minimized. Note that the optimal CRC can be different for different values of  $k$ . If the SNR is not sufficiently high, the CRC polynomial that minimizes the union bound in (22) may not minimize the actual  $P_{e,\lambda}$ .

Nevertheless, when SNR is sufficiently high or equivalently if the target probability of UE  $P_{e,\lambda}$  is sufficiently low (typically less than  $10^{-6}$ ), the union bound (22) will be dominated by its first term  $C_{d_{\min}^l} Q(A\sqrt{d_{\min}^l})$ , which becomes asymptotically tight to  $P_{e,\lambda}$ . Furthermore, in most cases at high SNR where the operating  $A$  is large enough, the first active term in (22) is only dominated by  $d_{\min}^l$ . The following theorem justifies this statement.

**Theorem 1.** *For a given higher-rate code  $\mathcal{C}_h$ , let  $C_{d_{\min,1}^l}, \dots, C_n$  and  $C'_{d_{\min,2}^l}, \dots, C'_n$  be two distance spectra of lower-rate codes generated by CRC polynomials  $p_1(x)$  and  $p_2(x)$ . If  $d_{\min,1}^l < d_{\min,2}^l$ , there exists a positive threshold  $A^*$  such that if  $A > A^*$ ,*

$$\sum_{d=d_{\min,1}^l}^n C_d Q(A\sqrt{d}) > \sum_{d=d_{\min,2}^l}^n C'_d Q(A\sqrt{d}). \quad (25)$$

*In the special case where  $d_{\min,1}^l = d_{\min,2}^l$  and  $C_{d_{\min,1}^l} > C'_{d_{\min,1}^l}$ , the above inequality still holds.*

*Proof:* Assume that  $d_{\min,1}^l < d_{\min,2}^l$ . Since all coefficients  $C_d, C'_d$  are positive and bounded,

$$\lim_{A \rightarrow \infty} \frac{\sum_{d=d_{\min,1}^l}^n C_d Q(A\sqrt{d})}{\sum_{d=d_{\min,2}^l}^n C'_d Q(A\sqrt{d})} \quad (26)$$

$$\begin{aligned} &= \lim_{A \rightarrow \infty} \frac{C_{d_{\min,1}^l} \exp(-\frac{A^2 d_{\min,1}^l}{2})}{C'_{d_{\min,2}^l} \exp(-\frac{A^2 d_{\min,2}^l}{2})} \\ &\quad \cdot \frac{[1 + \sum_{d=d_{\min,1}^l+1}^n \frac{C_d}{C_{d_{\min,1}^l}} \exp(-\frac{A^2(d-d_{\min,1}^l)}{2})]}{[1 + \sum_{d=d_{\min,2}^l+1}^n \frac{C'_d}{C'_{d_{\min,2}^l}} \exp(-\frac{A^2(d-d_{\min,1}^l)}{2})]} \end{aligned} \quad (27)$$

$$\begin{aligned} &= \lim_{A \rightarrow \infty} \frac{C_{d_{\min,1}^l}}{C'_{d_{\min,2}^l}} \exp\left(\frac{A^2}{2}(d_{\min,2}^l - d_{\min,1}^l)\right) \\ &= \infty. \end{aligned} \quad (28)$$

Hence, there exists a threshold  $A^*$  such that when  $A > A^*$ ,  $\sum_{d=d_{\min,1}^l}^n C_d Q(A\sqrt{d}) > \sum_{d=d_{\min,2}^l}^n C'_d Q(A\sqrt{d})$ . In the special case where  $d_{\min,1}^l = d_{\min,2}^l$  and  $C_{d_{\min,1}^l} > C'_{d_{\min,1}^l}$ , the limit in (28) is still greater than 1. ■

For sufficiently low target  $P_{e,\lambda}$ , the operating amplitude  $A$  is typically large enough such that  $A > A^*$  is easily met in practice. In these common situations, the DSO CRC design principle reduces to maximizing the minimum distance  $d_{\min}^l$  of the resulting CRC-CC concatenated code.

As an illustrative example, Fig. 2 shows the union bound (22) for two degree-5 CRC polynomials among the 16 candidates for  $k = 10$  and ZTCC (13, 17). The CRC 0x3B minimizes the union bound at low SNR, but the CRC 0x2D minimizes the union bound at high SNR. A detailed computation reveals that  $d_{\min}^l = 11$ ,  $C_{d_{\min}^l} = 17$  for 0x3B, and  $d_{\min}^l = 12$ ,  $C_{d_{\min}^l} = 76$  for 0x2D. Thus, the DSO CRC may not necessarily have the best minimum distance. In this example, the threshold at which the DSO CRC polynomial switches from 0x3B to 0x2D is  $-0.2398$  dB. However, the gap between the performance of the two CRC polynomials is minimal, especially at low SNR.

For a given CC and a specified CRC degree  $m$ , one may ask: how large can  $d_{\min}^l$  be? The next theorem gives a tight upper bound on  $d_{\min}^l$  in terms of the distance spectrum of the higher-rate code  $\mathcal{C}_h$ .

**Theorem 2.** *Given a specified CRC degree  $m$  and a higher-rate code  $\mathcal{C}_h$  with distance spectrum  $B_1, \dots, B_n$ , define  $w^*$  as the minimum distance at which  $\sum_{d=1}^w B_d \geq 2^m$ . For any degree- $m$  CRC polynomial, we have  $d_{\min}^l \leq 2w^*$ .*

*Proof:* Define the set  $V(\mathbf{c})$  to be the set of codewords from the higher-rate code  $\mathcal{C}_h$  that unambiguously decode to codeword  $\mathbf{c}$  of the lower-rate code  $\mathcal{C}_l$ . Specifically, for each  $\mathbf{c} \in \mathcal{C}_l$ , define

$$V(\mathbf{c}) \triangleq \{\mathbf{r} \in \mathcal{C}_h : d_H(\mathbf{r}, \mathbf{c}) < d_H(\mathbf{r}, \mathbf{c}'), \forall \mathbf{c}' \in \mathcal{C}_l\}. \quad (29)$$

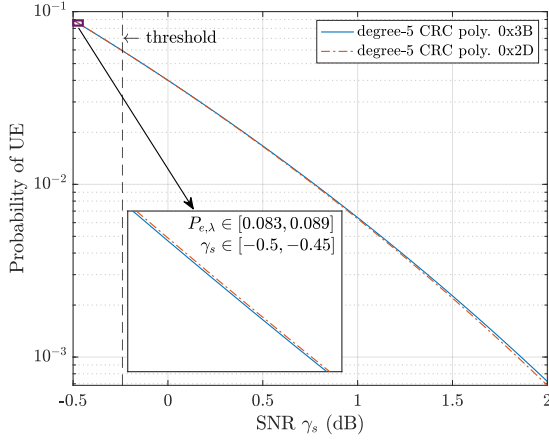


Fig. 2. Comparison of the DSO CRC polynomials for  $k = 10$ ,  $m = 5$  and ZTCC (13, 17). The blocklength  $n = 36$ . The threshold value is  $-0.2398$  dB.

Hence, by linearity of the higher-rate code, the cardinality of  $V(c)$  for every  $c \in \mathcal{C}_l$  is exactly the same. Hence,

$$|V(c)| \leq \frac{|\mathcal{C}_h|}{|\mathcal{C}_l|} = 2^m, \quad (30)$$

where (30) is an inequality because some codewords  $\mathbf{r} \in \mathcal{C}_h$  may be equidistant from two or more lower-rate codewords.

Next, we show that for a given  $c \in \mathcal{C}_l$ ,  $d_H(\mathbf{r}, c) < \frac{1}{2}d_{\min}^l$  implies that  $\mathbf{r} \in V(c)$ . By definition of the minimum distance, for two arbitrary distinct codewords  $c, c' \in \mathcal{C}_l$ ,  $d_H(c, c') \geq d_{\min}^l$ . Hence, for any  $\mathbf{r} \in \mathcal{C}_h$ , by triangle inequality,

$$d_H(\mathbf{r}, c) + d_H(\mathbf{r}, c') \geq d_H(c, c') \geq d_{\min}^l. \quad (31)$$

Thus, if  $d_H(\mathbf{r}, c) < \frac{1}{2}d_{\min}^l$ , this implies that  $d_H(\mathbf{r}, c') > \frac{1}{2}d_{\min}^l$  for any other  $c' \in \mathcal{C}_l$ , i.e.,  $d_H(\mathbf{r}, c) < d_H(\mathbf{r}, c')$  for all  $c' \in \mathcal{C}_l$ . By definition of  $V(c)$ , we conclude that  $\mathbf{r} \in V(c)$ .

By law of contraposition, if  $\mathbf{r} \notin V(c)$ , then  $d_H(\mathbf{r}, c) \geq \frac{1}{2}d_{\min}^l$ . Indeed, when  $\sum_{d=1}^w B_d \geq 2^m$  (i.e.,  $\sum_{d=0}^w B_d \geq 2^m + 1$ ), by pigeonhole principle, there exists a codeword  $\mathbf{r} \in \mathcal{C}_h$  that is outside of  $V(c)$  and whose distance from  $c$  satisfies  $d_H(\mathbf{r}, c) \leq w$ . Therefore, for this codeword  $\mathbf{r}$ ,  $w \geq d_H(\mathbf{r}, c) \geq \frac{1}{2}d_{\min}^l$  or equivalently,  $d_{\min}^l \leq 2d_H(\mathbf{r}, c) \leq 2w$ . Since this holds for any  $w$  for which  $\sum_{d=1}^w B_d \geq 2^m$ , it suffices to consider the minimum such value  $w^*$ . ■

Table I shows the comparison between  $d_{\min}^l$  and the upper bound in Theorem 2 for both ZTCC and TBCC of rate-1/2 convolutional generator (13, 17). We see that the proposed bound is sharp since some DSO CRC polynomials achieve the upper bound.

### B. A Two-Phase DSO CRC Design Algorithm for TBCCs

We focus on finding the DSO CRC polynomial for low target  $P_{e,\lambda}$ . As discussed earlier, the design principle under this circumstance conveniently reduces to maximizing the  $d_{\min}^l$  of the lower-rate code. Thus, the optimal CRC polynomial depends on the CC but not the SNR.

In principle, the DSO CRC design algorithm comprises a *collection phase* that gathers error events of the higher-rate code  $\mathcal{C}_h$  up to a certain distance  $\tilde{d}$ , and a *search phase*

TABLE I  
COMPARISON BETWEEN  $d_{\min}^l$  OF THE DSO CRC POLYNOMIAL AND  $2w^*$  COMPUTED FROM THEOREM 1 FOR  $k = 64$

$m$	ZTCC (13, 17)			TBCC (13, 17)		
	$p(x)$	$d_{\min}^l$	$2w^*$	$p(x)$	$d_{\min}^l$	$2w^*$
0	0x1	6	12	0x1	6	12
3	0x9	10	12	0xF	8	12
4	0x1B	10	12	0x1F	9	12
5	0x2D	12	12	0x2D	10	12
6	0x43	12	12	0x63	12	12
7	0xB5	13	14	0xED	12	14
8	0x107	14	14	0x107	12	14
9	0x313	14	16	0x349	14	16
10	0x50B	15	18	0x49D	14	18

that identifies the degree- $m$  DSO CRC polynomial using the error events gathered in the collection phase. In this section, we propose a two-phase DSO CRC design algorithm particularized to TBCCs of arbitrary rate (including rate  $1/\omega$ ). Later, we point out that our algorithm is also applicable to ZTCCs of arbitrary rate with a few distinctions.

The difficulty of designing DSO CRC polynomials for TB trellises lies in the fact that a TB trellis is a union of  $2^\nu$  subtrellises that share trellis branches in the middle. Thus, to collect error events that meet the TB condition, a straightforward collection method is to perform Viterbi algorithm separately on each possible start state to identify the *irreducible error event* (IEE) that leaves the start state once and rejoins it once, and then use them to reconstruct length- $N$  TB paths with distance less than  $\tilde{d}$ , which are the error events of interest for the higher-rate code. However, this scheme will be *inefficient* in that for each nonzero start state, there exists a catastrophic IEE that spends a majority of time in the self-loop of the zero state. Such an IEE has the catastrophic property that its length grows unbounded with a finite weight. As a consequence, they are rarely used during reconstruction yet occupy a significant portion of total IEEs.

The algorithm we are about to propose follows the straightforward algorithm with the distinction in collecting IEEs. To circumvent the aforementioned inefficiency, we wish to identify IEEs whose weight is proportional to its length. To this end, we first partition the TB trellis into several sets that are closed under cyclic shifts. Next, all elements in each set are reconstructed via the concatenation of the corresponding IEEs and circular shifts of the resulting path.

For a given length- $N$  TB trellis associated with a minimal convolutional encoder  $\mathbf{g}(x)$ , let  $V_0 = \{0, 1, \dots, 2^\nu - 1\}$  be the set of possible encoder states. We seek a partition of TB trellis, i.e., mutually exclusive sets that, together, contain all length- $N$  TB paths. To do this, we define  $\text{TBP}(0)$  as the set that contains all TB paths that traverse through state 0;  $\text{TBP}(1)$  contains the TB paths that traverse through state 1 but not state 0; so on and so forth. In general, the set  $\text{TBP}(\sigma)$  for  $\sigma \in V_0$  is defined as follows:

$$\begin{aligned} \text{TBP}(\sigma) &\triangleq \{(s, \mathbf{a}) \in V_0^{N+1} \times \mathcal{A}^N : s_0 = s_N; \\ &\exists i \in \mathcal{I} \text{ s.t. } s_i = \sigma; \forall i \in \mathcal{I}, s_i \notin \{0, 1, \dots, \sigma - 1\}\}. \end{aligned} \quad (32)$$

An important property of the above decomposition is that each set  $\text{TBP}(\sigma)$  is closed under cyclic shifts, as circularly

shifting a TB path preserves the sequence of states through which it traverses. Furthermore, such a partition of TB trellis motivates the following IEE.

**Definition 2** (Irreducible error events). *For a TB trellis  $T$  on sequential time axis  $\mathcal{I} = \{0, 1, \dots, N\}$ , the set of irreducible error events  $(s, \mathbf{a})$  at state  $\sigma \in V_0$  is defined as*

$$\text{IEE}(\sigma) \triangleq \bigcup_{i=1,2,\dots,N} \overline{\text{IEE}}(\sigma, i), \quad (33)$$

where

$$\overline{\text{IEE}}(\sigma, i) \triangleq \{(s, \mathbf{a}) \in V_0^{i+1} \times \mathcal{A}^i : s_0 = s_i = \sigma; \forall j, 0 < j < i, s_j \notin \{0, 1, \dots, \sigma\}\}. \quad (34)$$

For ZTCCs, Lou *et al.* [28] considered finding IEEs that start and end at the zero state and counting the allowed combinations. Hence, The IEE defined above generalizes Lou *et al.*'s IEEs. Since for a nonzero start state, no IEE can traverse the zero state, this guarantees that the weight of the IEE grows proportionally with its length, thus avoiding the inefficiency incurred in the straightforward algorithm.

With the sets  $\text{TBP}(\sigma)$  defined as above, the following theorem describes how to efficiently find all elements in each  $\text{TBP}(\sigma)$  via the corresponding IEEs.

**Theorem 3.** *Every TB path  $(s, \mathbf{a}) \in \text{TBP}(\sigma)$  can be constructed from the IEEs in  $\text{IEE}(\sigma)$  via concatenation and subsequent cyclic shifts.*

*Proof:* Let us consider  $T$  as a TB trellis defined on a sequential time axis  $\mathcal{I} = \{0, 1, \dots, N\}$ . For any TB path  $(s, \mathbf{a}) \in \text{TBP}(\sigma)$  of length  $N$  on  $T$ , we can first circularly shift it to some other TB path  $(s^{(0)}, \mathbf{a}^{(0)}) \in \text{TBP}(\sigma)$  on  $T$  such that  $s_0^{(0)} = s_N^{(0)} = \sigma$ .

Now, we examine  $s^{(0)}$  over  $\mathcal{I}$ . If  $s^{(0)}$  is already an element of  $\text{IEE}(\sigma)$ , then there is nothing to prove. Otherwise, there exists a time index  $j$ ,  $0 < j < N$ , such that  $s_j = \sigma$ . In this case, we break the TB path  $(s^{(0)}, \mathbf{a}^{(0)})$  at time  $j$  into two sub-paths  $(s^{(1)}, \mathbf{a}^{(1)})$  and  $(s^{(2)}, \mathbf{a}^{(2)})$ , where

$$\begin{aligned} s^{(1)} &= (s_0, s_1, \dots, s_j), \quad \mathbf{a}^{(1)} = (a_0, a_1, \dots, a_{j-1}), \\ s^{(2)} &= (s_j, s_{j+1}, \dots, s_N), \quad \mathbf{a}^{(2)} = (a_j, a_{j+1}, \dots, a_{N-1}). \end{aligned}$$

Note that after segmentation of  $(s^{(0)}, \mathbf{a}^{(0)})$ , the resultant two sub-paths,  $(s^{(1)}, \mathbf{a}^{(1)})$  and  $(s^{(2)}, \mathbf{a}^{(2)})$ , still meet the TB condition. Repeat the above procedure on  $(s^{(1)}, \mathbf{a}^{(1)})$  and  $(s^{(2)}, \mathbf{a}^{(2)})$ . Since the length of a new sub-path is strictly decreasing after each segmentation, the boundary case is the atomic sub-path  $(s, \mathbf{a})$  of some length  $j^*$  satisfying  $s_0 = s_{j^*} = \sigma$ ,  $s_{j'} \neq \sigma$ ,  $\forall j' \in (0, j^*)$ . Clearly, this atomic path is an element of  $\text{IEE}(\sigma)$ . Thus, we successfully decompose a length- $N$  TB path into elements of  $\text{IEE}(\sigma)$ . Hence, reversing the above procedure will turn elements of  $\text{IEE}(\sigma)$  into a length- $N$  TB path. ■

We now present our two-phase DSO CRC polynomial design algorithm for rate- $1/\omega$  TBCCs that consists of the collection procedure as described in Algorithm 1 and the search procedure as described in Algorithm 2. The algorithm can be easily extended to TBCCs of arbitrary rate. In the

---

#### Algorithm 1 The Collection Procedure

---

**Input:** The TB trellis  $T$ , threshold  $\tilde{d}$

**Output:** The list of IEEs  $\mathcal{L}_{\text{IEE}}(\tilde{d}) = \{(s, \mathbf{a}, \mathbf{v})\}$

- 1: Initialize lists  $\mathcal{L}_\sigma$  to be empty for all  $\sigma \in V_0$ ;
  - 2: **for**  $\sigma \leftarrow 0, 1, \dots, |V_0| - 1$  **do**
  - 3:     Perform Viterbi search at  $\sigma$  on  $T$  to collect list  $\mathcal{L}_\sigma(\tilde{d})$  of all IEEs of distances less than  $\tilde{d}$ ;
  - 4: **end for**
  - 5: **return**  $\mathcal{L}_{\text{IEE}}(\tilde{d}) \leftarrow \bigcup_{\sigma \in V_0} \mathcal{L}_\sigma(\tilde{d})$ ;
- 

---

#### Algorithm 2 The Search Procedure

---

**Input:** The trellis length  $N$ , degree  $m$ , list of IEEs  $\mathcal{L}_{\text{IEE}}(\tilde{d})$

**Output:** The optimal degree- $m$  CRC gen. poly.  $p(x)$

- 1: Initialize the list  $\mathcal{L}_{\text{CRC}}$  of  $2^{m-1}$  CRC candidates and empty lists  $\mathcal{L}_{\text{TBP}}(d)$  of TBPs,  $d = 1, \dots, \tilde{d} - 1$ ;
  - 2: **for**  $d \leftarrow 1, 2, \dots, \tilde{d} - 1$  **do**
  - 3:     Construct all TBPs  $(s, \mathbf{a}, \mathbf{v})$  from  $\mathcal{L}_{\text{IEE}}(\tilde{d})$  s.t.  $w_H(\mathbf{a}) = d$ ,  $|\mathbf{v}| = N$ , via concatenation and cyclic shifts;
  - 4:     For each TBP,  $\mathcal{L}_{\text{TBP}}(d) \leftarrow \mathcal{L}_{\text{TBP}}(d) \cup \{(s, \mathbf{a}, \mathbf{v})\}$ ;
  - 5: **end for**
  - 6:  $\text{Candi}(1) \leftarrow \mathcal{L}_{\text{CRC}}$ ;
  - 7: **for**  $d \leftarrow 1, \dots, \tilde{d} - 1$  **do**
  - 8:     **for**  $p_i(x) \in \text{Candi}(d)$  **do**
  - 9:         Pass all  $\mathbf{v}(x) \in \mathcal{L}_{\text{TBP}}(d)$  to  $p_i(x)$ ;
  - 10:          $C^{(i)} \leftarrow$  the number of divisible  $\mathbf{v}(x)$  of dist.  $d$ ;
  - 11:     **end for**
  - 12:      $C^* \leftarrow \min_{i \in \text{Candi}(d)} C^{(i)}$
  - 13:      $\text{Candi}(d+1) \leftarrow \{p_i(x) \in \text{Candi}(d) : C^{(i)} = C^*\}$ ;
  - 14:     **if**  $|\text{Candi}(d+1)| = 1$  **then**
  - 15:         **return**  $\text{Candi}(d+1)$ ;
  - 16:     **end if**
  - 17: **end for**
- 

collection procedure,  $(s, \mathbf{a}, \mathbf{v})$  denotes the triple of states  $s$ , outputs  $\mathbf{a}$  and inputs  $\mathbf{v}$ , where the inputs  $\mathbf{v}$  are uniquely determined by state transitions  $s_i \rightarrow s_{i+1}$ ,  $i = 0, 1, \dots, N-1$ . The TB trellis considered in the collection procedure should set a sufficiently large trellis length so that IEEs with bounded distance  $\tilde{d}$  are fully collected. Once the collection procedure is done, one can reuse the collected IEEs in the search procedure for various trellis lengths. For a given higher-rate code  $\mathcal{C}_h$  and a specified CRC degree  $m$ , according to Theorem 2, it suffices to consider distance threshold  $\tilde{d} \leq 2w^* + 1$ , where  $w^*$  is the minimum weight determined in the theorem, to identify the degree- $m$  DSO CRC polynomial.

In the search procedure,  $|\mathbf{v}|$  denotes the length of  $\mathbf{v}$ . Steps from lines 2 to 4 use the IEEs to build all length- $N$  trellis paths with distance less than  $\tilde{d}$ . In practice, this can be accomplished through dynamic programming. Specifically, for a given state  $\sigma \in V_0$ , let  $\mathcal{L}_\sigma(w, l)$  denote the list of TB paths of weight  $w$  and length  $l$  with initial state  $\sigma$ ,  $0 \leq w < \tilde{d}$ ,  $1 \leq l \leq N$ . Then, the update rule of  $\mathcal{L}_\sigma(w, l)$  is as follows: given an IEE  $(s, \mathbf{a}, \mathbf{v}) \in \text{IEE}(\sigma)$  with  $w_H(\mathbf{a}) \leq w$  and  $|\mathbf{v}| < l$ ,

$$\mathcal{L}_\sigma(w, l) \leftarrow \mathcal{L}_\sigma(w, l) \cup \{\mathcal{L}_\sigma(w - w_H(\mathbf{a}), l - |\mathbf{v}|) \oplus (s, \mathbf{a}, \mathbf{v})\},$$

where  $\mathcal{L}_\sigma(w, l) \oplus (s, \mathbf{a}, \mathbf{v})$  denotes appending  $(s, \mathbf{a}, \mathbf{v})$  to the



TABLE II  
POPULAR RATE-1/2 ZTCCS AND THEIR DSO CRC POLYNOMIALS FOR  
 $k = 64$  AT SUFFICIENTLY LOW PROBABILITY OF UE  $P_{e,\lambda}$

$\nu$	ZTCC $\mathbf{g}(x)$	DSO CRC Polynomials							
		$m = 3$	4	5	6	7	8	9	10
3	(13, 17)	9	1B	2D	43	B5	107	313	50B
4	(27, 31)	F	15	33	4F	D3	13F	2AD	709
5	(53, 75)	9	11	25	49	EF	131	23F	73D
6	(133, 171)	F	1B	23	41	8F	113	2EF	629
7	(247, 371)	9	13	3F	5B	E9	17F	2A5	61D
8	(561, 753)	F	11	33	49	8B	19D	27B	4CF
9	(1131, 1537)	D	15	21	51	B7	1D5	20F	50D
10	(2473, 3217)	F	13	3D	5B	BB	105	20D	6BB

TABLE III  
POPULAR RATE-1/2 TBCCS AND THEIR DSO CRC POLYNOMIALS FOR  
 $k = 64$  AT SUFFICIENTLY LOW PROBABILITY OF UE  $P_{e,\lambda}$

$\nu$	TBCC $\mathbf{g}(x)$	DSO CRC Polynomials							
		$m = 3$	4	5	6	7	8	9	10
3	(13, 17)	F	1F	2D	63	ED	107	349	49D
4	(27, 31)	F	11	33	4F	B5	1AB	265	4D1
5	(53, 75)	9	11	3F	63	BD	16D	349	41B
6	(133, 171)	F	1B	3D	7F	FF	145	2BD	571
7	(247, 371)	F	11	33	63	EF	145	3A1	5D7
8	(561, 753)	F	11	33	7F	FF	1AB	301	4F5
9	(1131, 1537)	D	15	33	51	C5	1FF	349	583
10	(2473, 3217)	F	1B	33	79	BB	199	217	4DD

rear of each element in  $\mathcal{L}_\sigma(w, l)$ . The update rule inherently requires that  $w, l$  be enumerated in ascending order and  $w_H(\mathbf{a}), |\mathbf{v}|$  in descending order. Finally, the set of length- $N$  TB paths of distance less than  $\tilde{d}$  via direct concatenation are given by  $\bigcup_{\sigma \in V_0} \mathcal{L}_\sigma(\tilde{d}, N)$ . The rest of the TB paths are obtained by circularly shifting elements in  $\bigcup_{\sigma \in V_0} \mathcal{L}_\sigma(\tilde{d}, N)$ .

We remark that our algorithm can be generalized to ZTCCs of arbitrary rate with the following distinctions: the collection procedure only collects IEEs that start and terminate at the zero state; the search procedure only performs dynamic programming to reconstruct all ZT paths with the target trellis length and distances less than  $\tilde{d}$ ; termination tails of each ZT path should be removed before CRC verification. The MATLAB routines are available for ZTCCs [36] and for TBCCs [37].

Table II presents the CRC polynomials of degree  $m$  from 3 to 10 that maximize  $d_{\min}^l$  for CRC-ZTCC codes based on a family of popular rate-1/2 ZTCCs with constraint length  $v$  from 3 to 10 for  $k = 64$ . These polynomials are the DSO-CRCs for a sufficiently low  $P_{e,\lambda}$ . Table III presents the TBCC counterpart in the same setting. The code generated by the CRC polynomial and CC in above tables is our designed CRC-CC concatenated code. In Sec. V, we will present the performance and complexity trade-off of these codes.

#### IV. PERFORMANCE AND COMPLEXITY OF SLVD

This section explores the performance and complexity of SLVD. For a specified CRC-CC concatenated code, performance under SLVD is characterized by three probabilities:  $P_{c,\Psi}$ ,  $P_{e,\Psi}$  and  $P_{\text{NACK},\Psi}$ . The average decoding complexity of SLVD is a function of expected list rank  $E[L]$ . In order to understand the performance-complexity trade-off, we investigate how these quantities vary with system parameters including the SNR  $\gamma_s$  and the constrained maximum list size  $\Psi$ .

Geometrically speaking, the process of SLVD is to draw a list decoding sphere around the received sequence  $\mathbf{y}$  with an increasing radius until the sphere touches the closest lower-rate codeword. To formalize this procedure, let us consider the set of received sequences  $\mathbf{y} \in \mathbb{R}^n \setminus \mathcal{S}$  where  $\mathcal{S}$  is the probability-zero set defined by  $\mathcal{S} \triangleq \{\mathbf{y} \in \mathbb{R}^n : \exists \mathbf{c}_1, \mathbf{c}_2 \in \mathcal{C}_h \text{ s.t. } \|\mathbf{y} - \mathbf{x}(\mathbf{c}_1)\| = \|\mathbf{y} - \mathbf{x}(\mathbf{c}_2)\|\}$ . For every  $\mathbf{y} \in \mathbb{R}^n \setminus \mathcal{S}$ , let

$$\mathbf{c}_1(\mathbf{y}), \mathbf{c}_2(\mathbf{y}), \dots, \mathbf{c}_{|\mathcal{C}_h|}(\mathbf{y}) \quad (35)$$

be an enumeration of  $\mathcal{C}_h$  such that

$$\|\mathbf{y} - \mathbf{x}(\mathbf{c}_1(\mathbf{y}))\| < \|\mathbf{y} - \mathbf{x}(\mathbf{c}_2(\mathbf{y}))\| < \dots < \|\mathbf{y} - \mathbf{x}(\mathbf{c}_{|\mathcal{C}_h|}(\mathbf{y}))\|.$$

Using the above enumeration, we formally define the terminating list rank  $L(\mathbf{y})$  and the terminating distance  $d_t(\mathbf{y})$  for  $\mathbf{y}$  as follows:

$$L(\mathbf{y}) \triangleq \min\{s : \mathbf{c}_s(\mathbf{y}) \in \mathcal{C}_l\} \quad (36)$$

$$d_t(\mathbf{y}) \triangleq \min_{\mathbf{c} \in \mathcal{C}_l} \|\mathbf{y} - \mathbf{x}(\mathbf{c})\|. \quad (37)$$

Thus, the list decoding sphere of  $\mathbf{y}$  can be expressed as

$$\mathcal{B}_{\text{SLVD}}(\mathbf{y}) = \{\mathbf{c} \in \mathcal{C}_h : \|\mathbf{y} - \mathbf{x}(\mathbf{c})\| \leq d_t(\mathbf{y})\}. \quad (38)$$

Clearly,  $L(\mathbf{y}) = |\mathcal{B}_{\text{SLVD}}(\mathbf{y})|$ .

The concepts above are defined for each individual received point  $\mathbf{y} \in \mathbb{R}^n \setminus \mathcal{S}$ . Alternatively, we can also consider the decoding region  $\mathcal{Y}(\mathbf{c})$  (i.e., the Voronoi region) of each lower-rate codeword  $\mathbf{c} \in \mathcal{C}_l$ :

$$\mathcal{Y}(\mathbf{c}) \triangleq \{\mathbf{y} \in \mathbb{R}^n \setminus \mathcal{S} : \|\mathbf{y} - \mathbf{x}(\mathbf{c})\| < \|\mathbf{y} - \mathbf{x}(\mathbf{c}')\|, \forall \mathbf{c}' \in \mathcal{C}_l \setminus \{\mathbf{c}\}\}. \quad (39)$$

For SLVD, the decoding region  $\mathcal{Y}(\mathbf{c})$  can be further decomposed into finer subsets according to the list rank. Namely, for each  $\mathbf{c} \in \mathcal{C}_l$  and a particular list rank  $s \in [1, |\mathcal{C}_h| - |\mathcal{C}_l| + 1]$ ,

$$\begin{aligned} \mathcal{Z}_s(\mathbf{c}) \triangleq \{ & \mathbf{y} \in \mathbb{R}^n \setminus \mathcal{S} : \exists \mathbf{c}_1, \dots, \mathbf{c}_{s-1} \in \mathcal{C}_h \setminus \mathcal{C}_l \text{ s.t.} \\ & \|\mathbf{y} - \mathbf{x}(\mathbf{c})\| > \max_{j=1,2,\dots,s-1} \|\mathbf{y} - \mathbf{x}(\mathbf{c}_j)\| \text{ and} \\ & \|\mathbf{y} - \mathbf{x}(\mathbf{c})\| < \min_{\mathbf{c}' \notin \mathcal{C}_h \setminus \{\mathbf{c}, \mathbf{c}_1, \dots, \mathbf{c}_{s-1}\}} \|\mathbf{y} - \mathbf{x}(\mathbf{c}')\| \}. \end{aligned} \quad (40)$$

Here, each  $\mathcal{Z}_s(\mathbf{c})$  is referred to as the *order- $s$  decoding region of  $\mathbf{c}$* . Obviously, for each  $\mathbf{c} \in \mathcal{C}_l$ , we have

$$\mathcal{Z}_{s_1}(\mathbf{c}) \cap \mathcal{Z}_{s_2}(\mathbf{c}) = \emptyset, \quad \text{if } s_1 \neq s_2 \quad (41)$$

$$\mathcal{Y}(\mathbf{c}) = \bigcup_{s=1,2,\dots,|\mathcal{C}_h|-|\mathcal{C}_l|+1} \mathcal{Z}_s(\mathbf{c}). \quad (42)$$

By linearity of the code, the order- $s$  decoding regions of all lower-rate codewords are isomorphic. With BPSK modulation, the bisection hyperplane of any two codewords passes through the origin of  $\mathbb{R}^n$ , making each order- $s$  decoding region a polyhedron. Note that there exists a *supremum list rank*  $\lambda$

$$\lambda \triangleq \max\{s : \mathcal{Z}_s(\mathbf{c}) \neq \emptyset, \forall \mathbf{c} \in \mathcal{C}_l\}. \quad (43)$$

Here, the supremum list rank  $\lambda$  only depends on  $\mathcal{C}_l$  and  $\mathcal{C}_h$  and is independent of  $\Psi$ . Hence, if  $\Psi \geq \lambda$ , the possible outcomes of SLVD include only correct decoding or UE. Namely, NACKs are not possible.

### A. Performance Analysis

We first give our results on how  $P_{c,\Psi}$ ,  $P_{e,\Psi}$  and  $P_{NACK,\Psi}$  vary with  $\Psi$  for a fixed SNR. Each of these probabilities may be understood as the probability of an event defined as a set of received sequences  $\mathbf{y}$ . For example, with  $\bar{c} \in \mathcal{C}_l$  as the transmitted codeword, by linearity, we have

$$\begin{aligned} P_{c,\Psi} &= \mathbb{P} \left( \bigcup_{s=1,2,\dots,\Psi} \mathcal{Z}_s(\bar{c}) \middle| \mathbf{X} = \mathbf{x}(\bar{c}) \right) \\ &= \sum_{s=1}^{\Psi} \mathbb{P}(\mathcal{Z}_s(\bar{c}) | \mathbf{X} = \mathbf{x}(\bar{c})) \end{aligned} \quad (44)$$

$$\begin{aligned} P_{e,\Psi} &= \sum_{\mathbf{c} \in \mathcal{C}_l \setminus \{\bar{c}\}} \mathbb{P} \left( \bigcup_{s=1,2,\dots,\Psi} \mathcal{Z}_s(\mathbf{c}) \middle| \mathbf{X} = \mathbf{x}(\bar{c}) \right) \\ &= \sum_{s=1}^{\Psi} \sum_{\mathbf{c} \in \mathcal{C}_l \setminus \{\bar{c}\}} \mathbb{P}(\mathcal{Z}_s(\mathbf{c}) | \mathbf{X} = \mathbf{x}(\bar{c})). \end{aligned} \quad (45)$$

**Theorem 4.** For a given CC-CRC concatenated code decoded with SLVD at a fixed SNR,  $P_{c,\Psi}$  and  $P_{e,\Psi}$  are both strictly increasing in  $\Psi$  and will converge to  $P_{c,\lambda}$  and  $P_{e,\lambda}$  respectively, where  $P_{c,\lambda} + P_{e,\lambda} = 1$ .

*Proof:* According to (44) and (45),  $P_{c,\Psi}$  and  $P_{e,\Psi}$  are summations of order- $s$  decoding regions  $\mathbb{P}(\mathcal{Z}_s(\mathbf{c}) | \mathbf{X} = \mathbf{x}(\bar{c}))$ , thus are non-decreasing in  $\Psi$ . For each  $\mathbf{c} \in \mathcal{C}_l$  and  $s \leq \lambda$ ,  $\mathbb{P}(\mathcal{Z}_s(\mathbf{c}) | \mathbf{X} = \mathbf{x}(\bar{c}))$  is solely determined by the SNR value and is independent of  $\Psi$ . Since every order- $s$  decoding region  $\mathcal{Z}_s(\mathbf{c})$  is the intersection of halfplanes, it follows that each  $\mathcal{Z}_s(\mathbf{c})$  is an open set. Hence, it suffices to show that each  $\mathcal{Z}_s(\mathbf{c})$  is nonempty. To this end, we use induction to show that if  $\mathcal{Z}_s(\mathbf{c})$  is open and nonempty, so is  $\mathcal{Z}_{s-1}(\mathbf{c})$ .

By definition,  $\mathcal{Z}_\lambda(\mathbf{c})$  is open and nonempty. Assume  $\mathcal{Z}_s(\mathbf{c})$  is open and nonempty for some fixed  $s \leq \lambda$ . Hence, there exists  $\mathbf{y} \in \mathcal{Z}_s(\mathbf{c})$  with  $\mathbf{c}_1, \mathbf{c}_2, \dots, \mathbf{c}_s \in \mathcal{B}_{\text{SLVD}}(\mathbf{y})$ , where  $\mathbf{c}_1, \dots, \mathbf{c}_{s-1} \in \mathcal{C}_h \setminus \mathcal{C}_l$  and  $\mathbf{c}_s \in \mathcal{C}_l$ . Next, we show that with probability 1, a point  $\mathbf{y}'$  can be constructed from  $\mathbf{y}$  such that  $\mathbf{c}_1, \mathbf{c}_2, \dots, \mathbf{c}_{j-1}, \mathbf{c}_{j+1}, \dots, \mathbf{c}_{s-1}, \mathbf{c}_s \in \mathcal{B}_{\text{SLVD}}(\mathbf{y}')$  for some  $j \in [2, s-2]$ .

The new point  $\mathbf{y}'$  is constructed as  $\mathbf{y}' = \mathbf{y} + t(\mathbf{x}(\mathbf{c}_s) - \mathbf{y})$ , where  $t \in [0, 1]$ . Hence,

$$\|\mathbf{x}(\mathbf{c}_s) - \mathbf{y}'\| = (1-t)\|\mathbf{y} - \mathbf{x}(\mathbf{c}_s)\|. \quad (46)$$

Therefore, it is equivalent to showing that there exists  $t \in (0, 1)$  such that for some  $j \in [1, s-1]$ ,

$$\|\mathbf{y}' - \mathbf{x}(\mathbf{c}_j)\| > (1-t)\|\mathbf{y} - \mathbf{x}(\mathbf{c}_s)\| \quad (47)$$

$$\max_{i \neq j} \|\mathbf{y}' - \mathbf{x}(\mathbf{c}_i)\| < (1-t)\|\mathbf{y} - \mathbf{x}(\mathbf{c}_s)\|. \quad (48)$$

To this end, we show that the set of  $\mathbf{y}$  for which no such  $t$  exists has a probability of zero. First, consider function

$$F(t) \triangleq \max_{i=1,2,\dots,s-1} \|\mathbf{y}' - \mathbf{x}(\mathbf{c}_i)\| - (1-t)\|\mathbf{y} - \mathbf{x}(\mathbf{c}_s)\|.$$

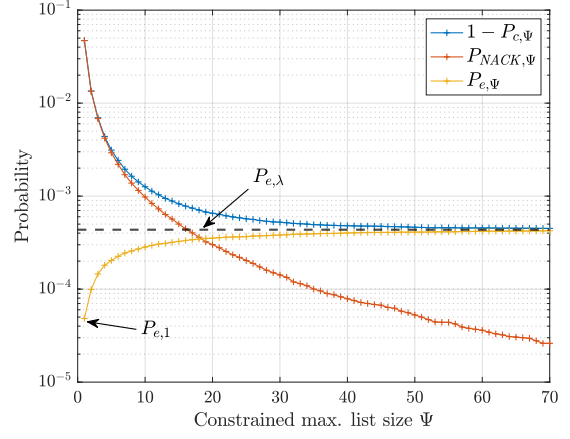


Fig. 3.  $1 - P_{c,\Psi}$ ,  $P_{NACK,\Psi}$ ,  $P_{e,\Psi}$  vs. the constraint maximum list size  $\Psi$  at SNR  $\gamma_s = 3$  dB for ZTCC (13, 17), degree-6 DSO CRC polynomial 0x43 and  $k = 64$  in Table II.

It can be shown that  $F(t)$  is a continuous function in  $t \in [0, 1]$ . Note that

$$F(0) = \max_{i=1,2,\dots,s-1} \|\mathbf{y} - \mathbf{x}(\mathbf{c}_i)\| - \|\mathbf{y} - \mathbf{x}(\mathbf{c}_s)\| < 0 \quad (49)$$

$$F(1) = \max_{i=1,2,\dots,s-1} \|\mathbf{x}(\mathbf{c}_s) - \mathbf{x}(\mathbf{c}_i)\| > 0. \quad (50)$$

By the intermediate value theorem, there exists a  $t^* \in (0, 1)$  such that

$$\max_{i=1,2,\dots,s-1} \|\mathbf{y}' - \mathbf{x}(\mathbf{c}_i)\| = (1-t^*)\|\mathbf{y} - \mathbf{x}(\mathbf{c}_s)\|. \quad (51)$$

Hence, the converse case can only occur if there exist two codewords  $\mathbf{c}_{j_1}$  and  $\mathbf{c}_{j_2}$ ,  $j_1 \neq j_2$ , such that

$$\|\mathbf{y}' - \mathbf{x}(\mathbf{c}_{j_1})\| = \|\mathbf{y}' - \mathbf{x}(\mathbf{c}_{j_2})\| = (1-t^*)\|\mathbf{y} - \mathbf{x}(\mathbf{c}_s)\|. \quad (52)$$

If (52) holds, this implies that  $\mathbf{y}'$  lies on the intersection of the hyperplane that bisects  $\mathbf{x}(\mathbf{c}_{j_1})\mathbf{x}(\mathbf{c}_s)$  and the hyperplane that bisects  $\mathbf{x}(\mathbf{c}_{j_2})\mathbf{x}(\mathbf{c}_s)$ . Namely,  $\mathbf{y}'$  lies on an  $(n-2)$ -dimensional hyperplane that crosses the origin. Hence, such  $\mathbf{y}'$  only occurs if line segment  $\mathbf{y}\mathbf{x}(\mathbf{c}_s)$  intersects with any of these  $(n-2)$ -dimensional hyperplanes. Therefore, the set of  $\mathbf{y}$  for which the converse case occurs is the union of finitely many  $(n-1)$ -dimensional hyperplanes, and thus has a probability of zero. Hence, we can construct a  $\mathbf{y}'$  from  $\mathbf{y} \in \mathcal{Z}_s(\mathbf{c})$  such that  $L(\mathbf{y}') = s-1$  with probability 1. Namely,  $\mathcal{Z}_{s-1}(\mathbf{c})$  is open and nonempty.

To summarize, every order- $s$  decoding region  $\mathcal{Z}_s(\mathbf{c})$  of  $\mathbf{c} \in \mathcal{C}_l$  with  $s \leq \lambda$  is open and nonempty. Thus,  $P_{c,\Psi}$  and  $P_{e,\Psi}$  are both strictly increasing in  $\Psi$  and will converge to  $P_{c,\lambda}$  and  $P_{e,\lambda}$  respectively provided that  $\Psi \geq \lambda$ . ■

As an example, Fig. 3 shows the probability of UE  $P_{e,\Psi}$  and probability of NACK  $P_{NACK,\Psi}$  vs. the constrained maximum list size  $\Psi$  for  $k = 64$ , degree-6 DSO CRC polynomial 0x43 and ZTCC (13, 17). It can be seen that  $P_{e,\Psi}$  quickly increases and converges to  $P_{e,\lambda}$  when  $\Psi$  is relatively small.

The proof of Theorem 4 implies that it is always possible to find a ray emitting from the BPSK-modulated point of a lower-rate codeword that traverses through all order- $s$  decoding

regions of that codeword. The monotone property of  $P_{e,\Psi}$  with  $\Psi$  indicates that for a fixed SNR value,

$$P_{e,1} \leq P_{e,\Psi} \leq P_{e,\lambda}, \quad \forall \Psi \in \mathbb{N}. \quad (53)$$

The proof of Theorem 4 also implies a property of the order- $\lambda$  decoding region  $\mathcal{Z}_\lambda(c)$ , namely that its closure must intersect with the boundary  $\partial\mathcal{Y}(c)$  of  $\mathcal{Y}(c)$ ,  $c \in \mathcal{C}_l$ . We formalize this in Theorem 5.

**Theorem 5.** *For any lower-rate codeword  $c \in \mathcal{C}_l$ ,  $\text{cl}(\mathcal{Z}_\lambda(c)) \cap \partial\mathcal{Y}(c) \neq \emptyset$ .*

*Proof:* Fix a lower-rate codeword  $c \in \mathcal{C}_l$ . Let  $\mathbf{y} \in \mathcal{Z}_\lambda(c)$ . Consider  $\mathbf{y}' = \mathbf{y} + t(\mathbf{y} - \mathbf{x}(c))$ ,  $t \geq 0$ . By the proof in Theorem 4, if  $\mathbf{y}' \in \mathcal{Y}(c)$ ,  $L(\mathbf{y}') \geq L(\mathbf{y}) = \lambda$ . Since  $\lambda$  is the maximum list rank,  $L(\mathbf{y}') = \lambda$  for all  $0 \leq t < t^*$ , where  $t^*$  is the threshold at which  $\mathbf{y}' \in \partial\mathcal{Y}(c)$ . This implies that  $\text{cl}(\mathcal{Z}_\lambda(c)) \cap \partial\mathcal{Y}(c) \neq \emptyset$ . ■

Theorem 5 indicates that one can find  $\lambda$  by following along the boundary of  $\mathcal{Y}(c)$  and making a slight deviations towards the decoding region  $\mathcal{Y}(c)$ . This approach is computationally challenging in  $\mathbb{R}^n$  for interesting values of  $n$ . While  $\lambda \leq |\mathcal{C}_h| - |\mathcal{C}_l| + 1$  provides an initial on  $\lambda$ , it remains an open problem to identify a tighter bound on  $\lambda$  and to develop an efficient algorithm to compute  $\lambda$ .

We next direct our attention to quantifying  $P_{e,1}$ ,  $P_{e,\lambda}$  in terms of the SNR (or equivalently in terms of amplitude  $A$ ) and the distance spectra of lower-rate code  $\mathcal{C}_l$  and higher-rate code  $\mathcal{C}_h$ .

**Theorem 6.** *Under SLVD decoding of a CC-CRC concatenated code with higher-rate distance spectrum  $B_{d_{\min}^h}, \dots, B_n$  and lower-rate distance spectrum  $C_{d_{\min}^l}, \dots, C_n$ ,*

$$P_{e,1} \leq \min \left\{ 2^{-m}, \sum_{d=d_{\min}^l}^n C_d Q(A\sqrt{d}) \right\} \quad (54)$$

$$\approx \min \left\{ 2^{-m}, C_{d_{\min}^l} Q(A\sqrt{d_{\min}^l}) \right\} \quad (55)$$

$$P_{e,\lambda} \leq \min \left\{ 1, \sum_{d=d_{\min}^l}^n C_d Q(A\sqrt{d}) \right\} \quad (56)$$

$$\approx \min \left\{ 1, \sum_{d=d_{\min}^l}^{\tilde{d}} C_d Q(A\sqrt{d}) \right\} \quad (57)$$

$$P_{NACK,1} \approx \min \left\{ 1 - 2^{-m}, \sum_{d=d_{\min}^h}^{\tilde{d}} B_d Q(A\sqrt{d}) - C_{d_{\min}^l} Q(A\sqrt{d_{\min}^l}) \right\}, \quad (58)$$

where the second approximation in braces in (55) is called the nearest neighbor approximation (NNA), and the second approximation in (57) is called the truncated union bound (TUB) at distance  $\tilde{d}$ .

*Proof:* First, note that  $P_{e,\Psi}$  is a monotonically decreasing function of  $A$  for any  $\Psi$ . This can be seen from (45) where as  $A$  increases, the center of the Gaussian density is moving away from every  $\mathbf{x}(c)$  for  $c \in \mathcal{C}_l \setminus \{\bar{c}\}$ . Hence, the corresponding

probability  $P(\mathcal{Z}_s(c)|\mathbf{X} = \mathbf{x}(\bar{c}))$  decreases with  $A$ , causing  $P_{e,\Psi}$  decreases with  $A$ .

Now we focus on the  $\Psi = 1$  case. The previous paragraph reveals that  $P_{e,1}$  has its maximum value at  $A = 0$ . As  $A \rightarrow 0$ , the transmitted point converges to the origin  $\mathbf{O}$  in  $\mathbb{R}^n$ . At the limit where  $\mathbf{x}(\bar{c}) = \mathbf{O}$ , the symmetry of the Gaussian density and linearity of the code ensures that each order-1 decoding region has a probability of  $2^{-(k+m)}$ . Hence,

$$P_{e,1} = \sum_{c \in \mathcal{C}_l \setminus \{\bar{c}\}} P(\mathcal{Z}_1(c)|\mathbf{X} = \mathbf{x}(\bar{c})) \quad (59)$$

$$\leq \lim_{A \rightarrow 0} \sum_{c \in \mathcal{C}_l \setminus \{\bar{c}\}} P(\mathcal{Z}_1(c)|\mathbf{X} = \mathbf{x}(\bar{c})) \quad (60)$$

$$= \sum_{c \in \mathcal{C}_l \setminus \{\bar{c}\}} P(\mathcal{Z}_1(c)|\mathbf{X} = \mathbf{O}) \quad (61)$$

$$= (2^k - 1)2^{-(k+m)} \leq 2^{-m}. \quad (62)$$

For any SNR value,  $P_{e,1} < P_{e,\lambda}$  so that the union bound (22) is also an upper bound for  $P_{e,1}$ . Hence, the minimum between the two is an upper bound on  $P_{e,1}$ . As SNR increases, the majority of probability will concentrate on the nearest neighbors of  $\bar{c}$ , hence, we can approximate  $P_{e,1}$  only using the nearest neighbors.

For  $P_{e,\lambda}$ , we upper bound it by the union bound (22). For ease of computation, we can consider the TUB up to a sufficient distance  $\tilde{d}$  to approximate the original union bound.

For  $P_{NACK,1}$ , in the extremely low SNR regime,  $P_{c,1} = 2^{-(k+m)}$  and  $P_{e,1} = 2^{-m}(1 - 2^{-k})$ . It follows that

$$P_{NACK,1} = 1 - P_{e,1} - P_{c,1} = 1 - 2^{-m}. \quad (63)$$

For arbitrary SNR, we have the union bound on  $P_{NACK,1} + P_{e,1}$ ,

$$P_{NACK,1} + P_{e,1} \leq \sum_{d=d_{\min}^h}^n B_d Q(A\sqrt{d}) \approx \sum_{d=d_{\min}^h}^{\tilde{d}} B_d Q(A\sqrt{d}).$$

Hence,

$$P_{NACK,1} \approx \sum_{d=d_{\min}^h}^{\tilde{d}} B_d Q(A\sqrt{d}) - C_{d_{\min}^l} Q(A\sqrt{d_{\min}^l}). \quad (64)$$

This concludes the entire proof. ■

Fig. 4 shows simulation results and the approximations for the three quantities addressed in Theorem 6:  $P_{NACK,1}$  and the lower and upper limits of  $P_{e,\Psi}$ , i.e.,  $P_{e,1}$  and  $P_{e,\lambda}$ . As SNR increases, all three approximations become asymptotically tight to the respective  $P_{e,1}$ ,  $P_{NACK,1}$ , and  $P_{e,\lambda}$ . The NNA approximation of the union bound on  $P_{e,\lambda}$  eventually will become asymptotically tight for  $P_{e,\lambda}$ , but is a tight approximation for  $P_{e,1}$  at a much lower SNR.

## B. Analysis of the Expected List Rank

As a corollary of Theorem 4, for a fixed SNR value and  $\Psi < \lambda$ ,  $E[L]$  will strictly increase as  $\Psi$  gets large. In the subsequent analysis, we assume that  $\Psi \geq \lambda$  and the terminating list rank  $L$  ranges from 1 to  $\lambda$  unless otherwise specified.

**Theorem 7.** *For a given CRC-CC concatenated code decoded with SLVD,  $\lim_{\gamma_s \rightarrow 0} E[L] = E[L|\mathbf{X} = \mathbf{O}]$ .*

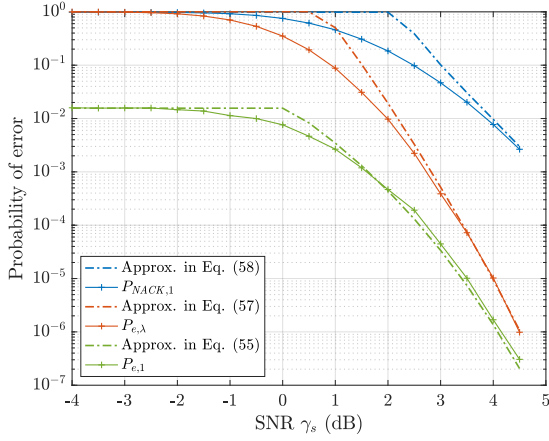


Fig. 4.  $P_{NACK,1}$ ,  $P_{e,\lambda}$  and  $P_{e,1}$  vs. SNR  $\gamma_s$  for ZTCC (13, 17), degree-6 DSO CRC polynomial 0x43 and  $k = 64$  in Table II. The TUB in (57) and (58) is obtained at  $\tilde{d} = 24$ .

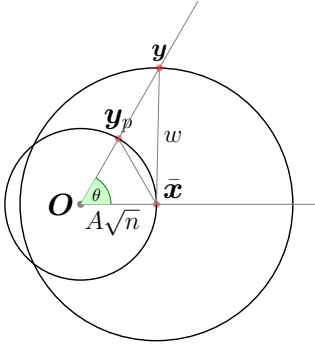


Fig. 5. An illustration of the projection method.

*Proof:* We use the projection method to show the convergence of  $E[L]$  in the low SNR regime.

For ease of discussion, let  $\mathcal{B}(a, r)$  denote the spherical surface of center  $a$  and radius  $r$  in  $\mathbb{R}^n$ . With BPSK modulation, all codewords sit on the *codeword sphere*  $\mathcal{B}(O, A\sqrt{n})$ , whereas the received point  $\mathbf{y}$  lies on the *noise sphere*  $\mathcal{B}(\bar{\mathbf{x}}, w)$  for some noise vector with Euclidean norm  $w$  added to the transmitted point  $\bar{\mathbf{x}}$ . The projection method projects the received point  $\mathbf{y}$  onto the codeword sphere. Namely, the projected point  $\mathbf{y}_p$  of  $\mathbf{y}$  is given by  $\mathbf{y}_p = (A\sqrt{n}/\|\mathbf{y}\|)\mathbf{y}$ . Fig. 5 illustrates the geometry of the projection method.

The significance of the projection method introduced above lies in the fact that it preserves the order of list decoded codewords. By law of cosines at angle  $\theta$  in Fig. 5, we obtain

$$\|\mathbf{y}_p - \bar{\mathbf{x}}\| = \begin{cases} \sqrt{\frac{\|\mathbf{y} - \bar{\mathbf{x}}\|^2 - \|\mathbf{y} - \mathbf{y}_p\|^2}{1 + \frac{\|\mathbf{y} - \mathbf{y}_p\|}{A\sqrt{n}}}}, & \text{if } \mathbf{y}_p \text{ in between } O, \mathbf{y} \\ \sqrt{\frac{\|\mathbf{y} - \bar{\mathbf{x}}\|^2 - \|\mathbf{y} - \mathbf{y}_p\|^2}{1 - \frac{\|\mathbf{y} - \mathbf{y}_p\|}{A\sqrt{n}}}}, & \text{if } \mathbf{y} \text{ in between } O, \mathbf{y}_p. \end{cases} \quad (65)$$

Hence, the monotone relation between  $\|\mathbf{y}_p - \bar{\mathbf{x}}\|$  and  $\|\mathbf{y} - \bar{\mathbf{x}}\|$  ensures that performing SLVD using  $\mathbf{y}$  is equivalent to that using  $\mathbf{y}_p$ . The essential motivation of projecting points onto the codeword sphere is to transfer the computation on the noise sphere to the codeword sphere.

To see how the projection method helps to show the convergence of  $E[L]$ , we first decompose the expected list rank  $E[L]$  according to the noise vector norm  $W = w$ . Namely,

$$\begin{aligned} E[L] &= E[L|\mathbf{X} = \bar{\mathbf{x}}] \\ &= \int_0^\infty f_W(w) E[L|W = w, \mathbf{X} = \bar{\mathbf{x}}] d\sigma, \end{aligned} \quad (66)$$

where  $\sigma$  is the spherical measure on  $\mathcal{B}(\bar{\mathbf{x}}, w)$  and  $f_W(w)$  denotes the density function of norm  $W = w$ . To find  $f_W(w)$ , let

$$\phi_n(w) \triangleq \frac{1}{(\sqrt{2\pi})^n} \exp\left(-\frac{w^2}{2}\right) \quad (67)$$

$$S_{n-1}(w) \triangleq \frac{2\pi^{\frac{n}{2}}}{\Gamma(\frac{n}{2})} w^{n-1} \quad (68)$$

be the  $n$ -dimensional standard normal density function and the spherical area of  $\mathcal{B}(\bar{\mathbf{x}}, w)$  in  $\mathbb{R}^n$ , respectively. Then,

$$f_W(w) = \phi_n(w) S_{n-1}(w) = \frac{w^{n-1}}{2^{\frac{n-2}{2}} \Gamma(\frac{n}{2})} \exp\left(-\frac{w^2}{2}\right). \quad (69)$$

For a given norm  $W = w$ , it follows that

$$E[L|W = w, \mathbf{X} = \bar{\mathbf{x}}] = \frac{1}{S_{n-1}(w)} \int_{\mathbf{y} \in \mathcal{B}(\bar{\mathbf{x}}, w) \setminus \mathcal{S}} L(\mathbf{y}) d\sigma. \quad (70)$$

Using the projection method, the integral in (70) can be shifted on the codeword sphere at the cost of introducing an induced density function  $g_w(\mathbf{y}_p)$ . Namely,

$$E[L|W = w, \mathbf{X} = \bar{\mathbf{x}}] = \int_{\mathbf{y}_p \in \mathcal{B}(O, A\sqrt{n}) \setminus \mathcal{S}} L(\mathbf{y}_p) g_w(\mathbf{y}_p) d\sigma. \quad (71)$$

In Appendix A, the induced density function, for  $w \geq A\sqrt{n}$ , is given by

$$g_w(\mathbf{y}_p) = \left(\frac{\|\mathbf{y}(\mathbf{y}_p)\|}{w}\right)^{n-1} \frac{1}{\cos \angle \bar{\mathbf{x}} \mathbf{y} O} \frac{1}{S_{n-1}(A\sqrt{n})}, \quad (72)$$

where  $\mathbf{y}(\mathbf{y}_p)$  is the pre-image of  $\mathbf{y}_p$  on the noise sphere  $\mathcal{B}(\bar{\mathbf{x}}, w)$ . Note that  $g_w(\mathbf{y}_p)$  is rotationally symmetric with respect to axis  $O\bar{\mathbf{x}}$ . Appendix A also shows that

$$g_w(\mathbf{y}_p) \geq \frac{1}{S_{n-1}(A\sqrt{n})} \left(1 - \frac{A\sqrt{n}}{w}\right)^{n-1} \quad (73)$$

$$g_w(\mathbf{y}_p) \leq \frac{1}{S_{n-1}(A\sqrt{n})} \left(1 + \frac{A\sqrt{n}}{w}\right)^{n-1}. \quad (74)$$

This implies that for a fixed norm  $w$ ,

$$\lim_{A \rightarrow 0} \frac{g_w(\mathbf{y}_p)}{(S_{n-1}(A\sqrt{n}))^{-1}} = 1. \quad (75)$$

Hence, for a fixed norm  $w$ , it follows that

$$\begin{aligned} \lim_{A \rightarrow 0} E[L|W = w, \mathbf{X} = \bar{\mathbf{x}}] &= \lim_{A \rightarrow 0} \int_{\mathbf{y}_p \in \mathcal{B}(O, A\sqrt{n}) \setminus \mathcal{S}} L(\mathbf{y}_p) g_w(\mathbf{y}_p) d\sigma \\ &= \lim_{A \rightarrow 0} \int_{\mathbf{y}_p \in \mathcal{B}(O, A\sqrt{n}) \setminus \mathcal{S}} L(\mathbf{y}_p) \frac{1}{S_{n-1}(A\sqrt{n})} d\sigma \end{aligned} \quad (76)$$

$$= \lim_{A \rightarrow 0} E[L|W = A\sqrt{n}, \mathbf{X} = O] \quad (77)$$

$$= E[L|\mathbf{X} = O], \quad (78)$$

$$= E[L|\mathbf{X} = O], \quad (79)$$

where we have used the fact that  $E[L|W = w, \mathbf{X} = \mathbf{O}] = E[L|\mathbf{X} = \mathbf{O}]$  for all  $w > 0$ . Similarly, we can also show that, for a fixed amplitude  $A$ ,

$$\lim_{w \rightarrow \infty} E[L|W = w, \mathbf{X} = \bar{\mathbf{x}}] = E[L|\mathbf{X} = \mathbf{O}]. \quad (80)$$

As a consequence,

$$\begin{aligned} \lim_{\gamma_s \rightarrow 0} E[L] &= \lim_{A \rightarrow 0} \int_0^\infty f_W(w) E[L|W = w, \mathbf{X} = \bar{\mathbf{x}}] dw \\ &= \int_0^\infty f(w) \lim_{A \rightarrow 0} E[L|W = w, \mathbf{X} = \bar{\mathbf{x}}] dw \\ &= \int_0^\infty f(w) E[L|\mathbf{X} = \mathbf{O}] dw \\ &= E[L|\mathbf{X} = \mathbf{O}]. \end{aligned} \quad (81)$$

This completes the proof.  $\blacksquare$

The proof above implies that in the low SNR regime, most of the probability will concentrate on the limit of  $E[L|W = w, \mathbf{X} = \bar{\mathbf{x}}]$  as  $w \rightarrow \infty$ , i.e.,  $E[L|\mathbf{X} = \mathbf{O}]$ . In general,  $E[L|\mathbf{X} = \mathbf{O}]$  depends on the geometric structure of the lower-rate code  $\mathcal{C}_l$  and the higher-rate code  $\mathcal{C}_h$  on  $\mathcal{B}(\mathbf{O}, A\sqrt{n})$  and it is not easy to obtain an analytic expression. Still, using a simple random coding argument, we show that a good concatenated code could achieve  $E[L|\mathbf{X} = \mathbf{O}] \leq 2^m$ .

**Lemma 1.** *For a given higher-rate code  $\mathcal{C}_h$  with  $|\mathcal{C}_h| = 2^{k+m}$ , let  $\mathcal{A}_l \triangleq \{\mathcal{C}' \subset \mathcal{C}_h : |\mathcal{C}'| = 2^k\}$ . Let  $P(\mathcal{C}') = \frac{1}{|\mathcal{A}_l|}$  be the uniform distribution defined over  $\mathcal{A}_l$ . Assume  $\mathcal{C}'$  is drawn according to  $P(\mathcal{C}')$ . Then,*

$$E_{\mathcal{C}'}[E[L|\mathbf{X} = \mathbf{O}, \mathcal{C}']] \leq 2^m. \quad (82)$$

*This implies that there exists a lower-rate code  $\mathcal{C}'$  (which may not be a linear code) such that  $E[L|\mathbf{X} = \mathbf{O}, \mathcal{C}'] \leq 2^m$ .*

*Proof:* Let  $L(\mathbf{y}, \mathcal{C}')$  be the list rank for received point  $\mathbf{y} \in \mathbb{R}^n$  when a lower-rate code is selected as  $\mathcal{C}' \in \mathcal{A}_l$ . Hence, we obtain

$$\begin{aligned} E_{\mathcal{C}'}[E[L|\mathbf{X} = \mathbf{O}, \mathcal{C}']] &= \sum_{\mathcal{C}' \in \mathcal{A}_l} P(\mathcal{C}') \frac{1}{S_{n-1}(A\sqrt{n})} \int_{\mathbf{y} \in \mathcal{B}(\mathbf{O}, A\sqrt{n})} L(\mathbf{y}, \mathcal{C}') d\sigma \\ &= \frac{1}{S_{n-1}(A\sqrt{n})} \int_{\mathbf{y} \in \mathcal{B}(\mathbf{O}, A\sqrt{n})} \sum_{\mathcal{C}' \in \mathcal{A}_l} P(\mathcal{C}') L(\mathbf{y}, \mathcal{C}') d\sigma \\ &= \frac{1}{S_{n-1}(A\sqrt{n})} \int_{\mathbf{y} \in \mathcal{B}(\mathbf{O}, A\sqrt{n})} E_{\mathcal{C}'}[L(\mathbf{y}, \mathcal{C}')|\mathbf{y}] d\sigma. \end{aligned} \quad (83)$$

Next, we show that for any  $\mathbf{y} \in \mathcal{B}(\mathbf{O}, A\sqrt{n})$ ,

$$E_{\mathcal{C}'}[L(\mathbf{y}, \mathcal{C}')|\mathbf{y}] \leq 2^m \quad (84)$$

for  $\mathcal{C}'$  uniformly drawn from  $\mathcal{A}_l$ . Fix a  $\mathbf{y} \in \mathcal{B}(\mathbf{O}, A\sqrt{n})$  and let  $\mathbf{c}_1(\mathbf{y}), \mathbf{c}_2(\mathbf{y}), \dots, \mathbf{c}_{|\mathcal{C}_h|}(\mathbf{y})$  be an enumeration of  $\mathcal{C}_h$  such that

$$\|\mathbf{y} - \mathbf{x}(\mathbf{c}_1(\mathbf{y}))\| \leq \dots \leq \|\mathbf{y} - \mathbf{x}(\mathbf{c}_{|\mathcal{C}_h|}(\mathbf{y}))\|.$$

Hence, the terminating list rank  $L(\mathbf{y}, \mathcal{C}')$  of  $\mathbf{y}$  is given by

$$L(\mathbf{y}, \mathcal{C}') = \min\{s : \mathbf{c}_s(\mathbf{y}) \in \mathcal{C}'\}. \quad (85)$$

<sup>2</sup>If there exist two codewords  $\mathbf{c}_{j_1}$  and  $\mathbf{c}_{j_2}$  that are equidistant from  $\mathbf{y}$ , the decoder adopts a pre-determined order relation between  $\mathbf{c}_{j_1}$  and  $\mathbf{c}_{j_2}$ .

For  $\mathcal{C}'$  uniformly drawn in  $\mathcal{A}_l$ , computing  $E_{\mathcal{C}'}[L(\mathbf{y}, \mathcal{C}')|\mathbf{y}]$  is equivalent to solving the following problem: there are  $|\mathcal{C}_h|$  balls in a basket, among which  $|\mathcal{C}'|$  of them are red and the rest are white. Balls are picked up  $|\mathcal{C}_h|$  times without replacement and the time at which the first red ball emerges is marked as the terminating list rank. Since every ordering of ball picking is equiprobable and is bijective with  $\mathcal{A}_l$ , the expected list rank in ball picking problem is equal to  $E_{\mathcal{C}'}[L(\mathbf{y}, \mathcal{C}')|\mathbf{y}]$ . Hence,

$$E_{\mathcal{C}'}[L(\mathbf{y}, \mathcal{C}')|\mathbf{y}] = \sum_{s=1}^{|\mathcal{C}_h| - |\mathcal{C}'| + 1} s \frac{\binom{|\mathcal{C}_h| - s}{|\mathcal{C}'| - 1}}{\binom{|\mathcal{C}_h|}{|\mathcal{C}'|}} \quad (86)$$

$$\begin{aligned} &= \frac{|\mathcal{C}_h| + 1}{|\mathcal{C}'| + 1} \\ &\leq 2^m, \end{aligned} \quad (87)$$

where (86) to (87) follows from a variant of the Chu-Vandermonde identity.  $\blacksquare$

In (66), it is shown that  $E[L]$  can be fully characterized by its conditional expectation  $E[L|W = w, \mathbf{X} = \bar{\mathbf{x}}]$ . For a given  $w$  and  $A$ , let  $\bar{\mathbf{x}}_e = \bar{\mathbf{x}}/A$  be the transmitted point with unit amplitude per dimension, it can be shown that

$$E[L|W = w, \mathbf{X} = \bar{\mathbf{x}}] = E[L|W = \eta, \mathbf{X} = \bar{\mathbf{x}}_e], \quad (88)$$

where  $\eta \triangleq w/A$  is called the *normalized norm*. Hence, it suffices to compute  $E[L|W = \eta, \mathbf{X} = \bar{\mathbf{x}}_e]$  and the SNR (i.e.,  $A$ ) only exhibits a scaling effect. To evaluate  $E[L|W = \eta, \mathbf{X} = \bar{\mathbf{x}}_e]$ , let  $\mathcal{C}_l^- \triangleq \mathcal{C}_l \setminus \{\bar{\mathbf{c}}\}$  and define the conditional probability of UE as

$$P_{e,\lambda}(\eta) \triangleq \sum_{\mathbf{c} \in \mathcal{C}_l^-} P(\mathcal{Y}(\mathbf{c})|W = \eta, \mathbf{X} = \bar{\mathbf{x}}_e). \quad (89)$$

In general, it is difficult to know the conditional probability of UE  $P_{e,\lambda}(\eta)$ . Assuming the knowledge of parametric information  $P_{e,\lambda}(\eta)$ , we first show an approximation that represents  $E[L|W = \eta, \mathbf{X} = \bar{\mathbf{x}}_e]$  as a linear combination between  $L = 1$  and  $L = \bar{L}$  with coefficient given by  $P_{e,\lambda}(\eta)$ .

**Approximation 3** (Parametric approximation). *For a CC-CRC concatenated code with corresponding parameters of  $\bar{L}$  and  $P_{e,\lambda}(\eta)$ , where  $\bar{L} \triangleq E[L|\mathbf{X} = \mathbf{O}]$ ,*

$$E[L|W = \eta, \mathbf{X} = \bar{\mathbf{x}}_e] \approx 1 - P_{e,\lambda}(\eta) + P_{e,\lambda}(\eta)\bar{L}. \quad (90)$$

Furthermore, applying transformation (97) yields the approximation of  $E[L]$ , i.e.,

$$E[L] \approx 1 - P_{e,\lambda} + P_{e,\lambda}E[L|\mathbf{X} = \mathbf{O}]. \quad (91)$$

*Proof:* For ease of discussion, we use the shorthand notation  $P(\cdot|\eta, \bar{\mathbf{x}}_e) \triangleq P(\cdot|W = \eta, \mathbf{X} = \bar{\mathbf{x}}_e)$  and  $P(\cdot|\mathbf{O}) =$

$P(\cdot|X = O)$ . Let us consider  $\eta$  for which  $P_{e,\lambda}(\eta) > 0$ . Hence,

$$\begin{aligned} & \mathbb{E}[L|W = \eta, X = \bar{x}_e] \\ &= \sum_{s=1}^{\lambda} sP(L = s|\eta, \bar{x}_e) \\ &= P(\mathcal{Y}(\bar{c})|\eta, \bar{x}_e) + \sum_{s=1}^{\lambda} sP(L = s|\eta, \bar{x}_e) - \sum_{s=1}^{\lambda} P(\mathcal{Z}_s(\bar{c})|\eta, \bar{x}_e) \\ &\geq 1 - P_{e,\lambda}(\eta) + \sum_{s=1}^{\lambda} s(P(L = s|\eta, \bar{x}_e) - P(\mathcal{Z}_s(\bar{c})|\eta, \bar{x}_e)) \\ &= 1 - P_{e,\lambda}(\eta) + P_{e,\lambda}(\eta) \left( \sum_{s=1}^{\lambda} s \frac{\sum_{c \in \mathcal{C}_l^-} P(\mathcal{Z}_s(c)|\eta, \bar{x}_e)}{\sum_{c \in \mathcal{C}_l^-} P(\mathcal{Y}(c)|\eta, \bar{x}_e)} \right) \end{aligned} \quad (92)$$

$$\approx 1 - P_{e,\lambda}(\eta) + P_{e,\lambda}(\eta) \left( \sum_{s=1}^{\lambda} sP(L = s|O) \right) \quad (93)$$

$$= 1 - P_{e,\lambda}(\eta) + P_{e,\lambda}(\eta)\bar{L},$$

where (92) to (93) follows from the substitution below. Consider the conditional list rank distribution

$$P_\eta = \left( \frac{\sum_{c \in \mathcal{C}_l^-} P(\mathcal{Z}_1(c)|\eta, \bar{x}_e)}{\sum_{c \in \mathcal{C}_l^-} P(\mathcal{Y}(c)|\eta, \bar{x}_e)}, \dots, \frac{\sum_{c \in \mathcal{C}_l^-} P(\mathcal{Z}_\lambda(c)|\eta, \bar{x}_e)}{\sum_{c \in \mathcal{C}_l^-} P(\mathcal{Y}(c)|\eta, \bar{x}_e)} \right). \quad (94)$$

Using the fact that  $\lim_{\eta \rightarrow \infty} g_\eta(\mathbf{y}_p) = 1/S_{n-1}(\sqrt{n})$ , the conditional list rank distribution  $P_\eta$  will converge to

$$\begin{aligned} P_\infty &= \left( \frac{P(\mathcal{Z}_1(c)|O)}{P(\mathcal{Y}(c)|O)}, \dots, \frac{P(\mathcal{Z}_\lambda(c)|O)}{P(\mathcal{Y}(c)|O)} \right) \\ &= \left( \frac{\sum_{c \in \mathcal{C}_l} P(\mathcal{Z}_1(c)|O)}{\sum_{c \in \mathcal{C}_l} P(\mathcal{Y}(c)|O)}, \dots, \frac{\sum_{c \in \mathcal{C}_l} P(\mathcal{Z}_\lambda(c)|O)}{\sum_{c \in \mathcal{C}_l} P(\mathcal{Y}(c)|O)} \right) \\ &= (P(L = 1|O), \dots, P(L = \lambda|O)), \end{aligned} \quad (95) \quad (96)$$

where  $c$  is any lower-rate codeword in (95). Hence, we directly replace  $P_\eta$  with the limit distribution  $P_\infty$  in (92). ■

Fig. 6 shows the simulation results of the conditional expected list rank  $\mathbb{E}[L|W = \eta, X = \bar{x}_e]$  vs. the normalized norm  $\eta$ . The corresponding parametric approximation is also given. We see that the parametric approximation exhibits a remarkable accuracy that improves as  $k$  increases. Observe that for large values of  $k$ , the convergent  $\mathbb{E}[L|W = \eta, X = \bar{x}_e]$  will be close to  $2^m$ .

Using the transformation

$$\mathbb{E}[L] = \int_0^\infty f_W(w) \mathbb{E}[L|W = (w/A), X = \bar{x}_e] dw, \quad (97)$$

we can produce  $\mathbb{E}[L]$  as a function of the SNR  $\gamma_s$ . Fig. 7 shows  $\mathbb{E}[L]$  vs. SNR along with its parametric approximations for ZTCC (13, 17) and various DSO CRC polynomials of degree  $m = 3, 4, \dots, 6$ . We see that the parametric approximation on  $\mathbb{E}[L]$  still remains extremely tight.

The parametric approximation provides a practically useful quantitative connection between performance and complexity. Specifically, for CRC-ZTCC codes with a target probability of UE  $P_{e,\lambda}^*$  and  $\bar{L} \approx 2^m$  for CRC degree  $m$ , (91) implies that a CRC with degree  $m \leq -\log(P_{e,\lambda}^*)$  is sufficient to maintain

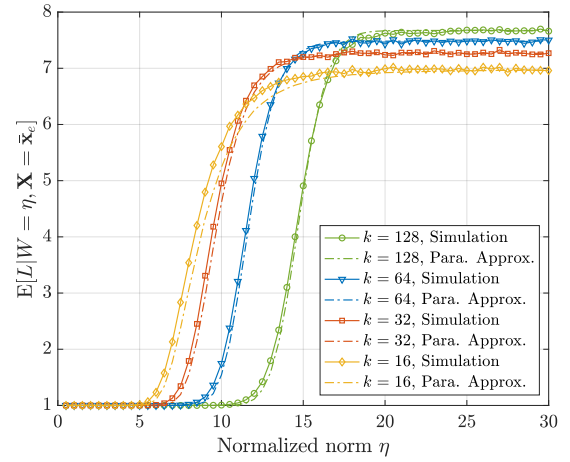


Fig. 6. The conditional expected list rank  $\mathbb{E}[L|W = \eta, X = \bar{x}_e]$  vs. the normalized norm  $\eta$  for degree-3 DSO CRC 0x9 and ZTCC (13, 17) for various information lengths  $k$ .

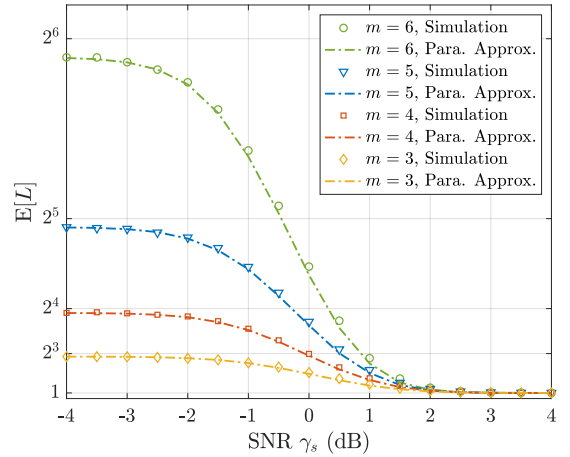


Fig. 7. The expected list rank  $\mathbb{E}[L]$  vs. SNR for various CRC-ZTCC codes and  $k = 64$ , where ZTCC is (13, 17) and the DSO CRC polynomials are from Table II with degree  $m = 3, 4, \dots, 6$ .

$\mathbb{E}[L] \leq 2$ , which ensures that the average complexity for SLVD to achieve  $P_{e,\lambda}^*$  is at most one more traceback than the classical Viterbi decoding.

As an alternative to Approximation 3, we provide a higher-order approximation formula for a good CRC-CC concatenated code that only requires knowledge of  $\mathbb{E}[L|X = O]$ . This alternative approximation is motivated by Shannon's observation [18] that an optimal  $(n, M)$  code places its codewords on the surface of a sphere such that the total solid angle  $\Omega_0$  is evenly divided among the  $M$  Voronoi regions, one for each codeword, and that each Voronoi region is a circular cone. Hence, if the CRC-CC concatenated code is good enough, both the decoding region  $\mathcal{Y}(c)$  and order-1 decoding region  $\mathcal{Z}_1(c)$  for a lower-rate codeword  $c \in \mathcal{C}_l$  should resemble circular cones.

For higher-order decoding regions  $\mathcal{Z}_s(c)$  with  $s \geq 1$ , their geometric shape in  $\mathbb{R}^n$  could be very complicated. In order to develop an approximation for  $\mathbb{E}[L|W = \eta, X = \bar{x}_e]$ , we propose the *onion model* for order-1 decoding region up to order- $\mu$  decoding region based on the following assumptions,



where  $\mu$  is a parameter to be optimized.

- 1) The union  $\bigcup_{i=1}^s \mathcal{Z}_i(\bar{c})$  of order-1 to order- $s$  decoding regions,  $1 \leq s \leq \mu$ , is also a circular cone with half angle  $\alpha_s$ . This implies that each order- $s$  decoding region,  $2 \leq s \leq \mu$  is an *annulus* in between two circular cones.
- 2) The solid angle  $\Omega(\alpha_s)$  of  $\bigcup_{i=1}^s \mathcal{Z}_i(\bar{c})$  is equal to  $\frac{s}{2^{k+m}} \Omega_0$ ,  $1 \leq s \leq \mu$ .
- 3) The conditional expected list rank beyond  $\bigcup_{i=1}^\mu \mathcal{Z}_i(\bar{c})$  is equal to  $\bar{L}$  (i.e.,  $E[L|\mathbf{X} = \mathbf{O}]$ ).

**Approximation 4** (Higher-order approximation). *For a given CRC-CC concatenated code, let  $\bar{L} = E[L|\mathbf{X} = \mathbf{O}]$ . With the aforementioned assumptions on parameter  $\mu$ ,  $\mu \in \mathbb{N}$ ,  $E[L|W = \eta, \mathbf{X} = \bar{\mathbf{x}}_e]$  is approximated by*

$$E[L|W = \eta, \mathbf{X} = \bar{\mathbf{x}}_e] \approx \begin{cases} 1, & \text{if } \eta < \sqrt{n} \sin \alpha_1 \\ \dots \\ s - \sum_{i=1}^{s-1} F_{\bar{\mathbf{x}}_e}(i), & \text{if } \sqrt{n} \sin \alpha_{s-1} \leq \eta < \sqrt{n} \sin \alpha_s \\ \dots \\ \bar{L} - (\bar{L} - \mu) F_{\bar{\mathbf{x}}_e}(\mu) - \sum_{i=1}^{\mu-1} F_{\bar{\mathbf{x}}_e}(i), & \text{if } \eta \geq \sqrt{n} \sin \alpha_\mu, \end{cases} \quad (98)$$

where

$$F_{\bar{\mathbf{x}}_e}(s) = \frac{\Gamma(\frac{n}{2})}{\sqrt{\pi} \Gamma(\frac{n-1}{2})} \left( \int_0^{\beta_{s,1}} \sin^{n-2} \theta d\theta + \int_0^{\beta_{s,2}} \sin^{n-2} \theta d\theta \right) \quad (99)$$

$$\beta_{s,1} = \frac{\pi}{2} + \alpha_s - \arcsin \left( \frac{\sqrt{\eta^2 - n \sin^2 \alpha_s}}{\eta} \right) \quad (100)$$

$$\beta_{s,2} = \left( \frac{\pi}{2} - \alpha_s - \arcsin \left( \frac{\sqrt{\eta^2 - n \sin^2 \alpha_s}}{\eta} \right) \right) \mathbf{1}_{\{\eta \leq \sqrt{n}\}}, \quad (101)$$

and  $\alpha_s$  is the half angle for which

$$\frac{\Omega(\alpha_s)}{\Omega_0} = \frac{\Gamma(\frac{n}{2})}{\sqrt{\pi} \Gamma(\frac{n-1}{2})} \int_0^{\alpha_s} \sin^{n-2} \theta d\theta = \frac{s}{2^{k+m}}. \quad (102)$$

*Proof:* The onion model assumptions implies that each higher order decoding region  $\mathcal{Z}_s(\bar{c})$ ,  $2 \leq s \leq \mu$ , is an annulus in between two circular cones. Hence,  $P(L = s|W = \eta, \mathbf{X} = \bar{\mathbf{x}}_e)$  is simply the spherical area of  $\mathcal{B}(\bar{\mathbf{x}}_e, \eta)$  cut out by the annulus. To evaluate this quantity, consider the cumulative probability function of  $L = s$ ,

$$F_{\bar{\mathbf{x}}_e}(s) \triangleq P(L \leq s, \hat{\mathbf{X}} = \bar{\mathbf{x}}_e). \quad (103)$$

Thus,

$$P(L = s|W = \eta, \mathbf{X} = \bar{\mathbf{x}}_e) = F_{\bar{\mathbf{x}}_e}(s) - F_{\bar{\mathbf{x}}_e}(s-1). \quad (104)$$

By the onion model assumptions, for  $\eta \geq \sqrt{n} \sin \alpha_\mu$ ,

$$E[L|W = \eta, \mathbf{X} = \bar{\mathbf{x}}_e] \quad (105)$$

$$\approx \sum_{i=1}^{\mu} i(F_{\bar{\mathbf{x}}_e}(i) - F_{\bar{\mathbf{x}}_e}(i-1)) + \bar{L}(1 - F_{\bar{\mathbf{x}}_e}(\mu)) \quad (106)$$

$$= \bar{L} - (\bar{L} - \mu) F_{\bar{\mathbf{x}}_e}(\mu) - \sum_{i=1}^{\mu-1} F_{\bar{\mathbf{x}}_e}(i). \quad (107)$$

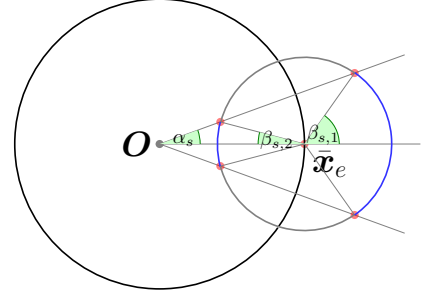


Fig. 8. The geometry of the cumulative probability function  $F_{\bar{\mathbf{x}}_e}(s)$ .

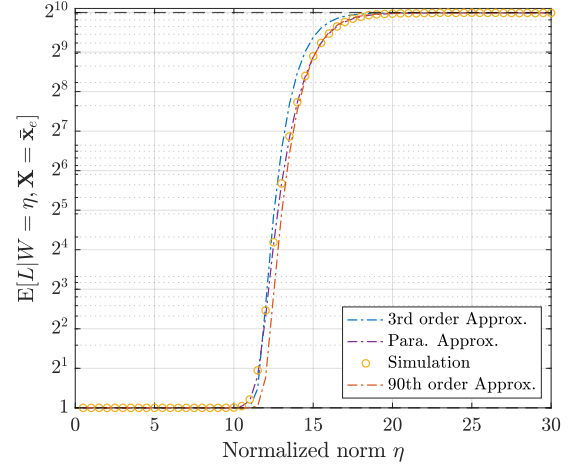


Fig. 9. The parametric and higher-order approximations of  $E[L|W = \eta, \mathbf{X} = \bar{\mathbf{x}}_e]$  for ZTCC (561, 753) used with the degree-10 DSO CRC polynomial 0x4CF at  $k = 64$ . Higher-order approximations assume the knowledge of  $\bar{L} = 1017$ .

In the similar fashion, for  $\sqrt{n} \sin \alpha_{s-1} \leq \eta < \sqrt{n} \sin \alpha_s$ ,  $1 \leq s \leq \mu$ ,

$$E[L|W = \eta, \mathbf{X} = \bar{\mathbf{x}}_e] \approx s - \sum_{i=1}^{s-1} F_{\bar{\mathbf{x}}_e}(i). \quad (108)$$

Next, we derive the cumulative probability function  $F_{\bar{\mathbf{x}}_e}(s)$ . Geometrically,  $F_{\bar{\mathbf{x}}_e}(s)$  is the fraction of the spherical area of  $\mathcal{B}(\bar{\mathbf{x}}_e, \eta)$  cut out by the circular cone  $\bigcup_{i=1}^s \mathcal{Z}_i(\bar{c})$  with half angle  $\alpha_s$  to the total noise spherical area. Fig. 8 shows the side view of this scenario in  $\mathbb{R}^3$ , in which the blue arc represents the spherical area contained in  $\bigcup_{i=1}^s \mathcal{Z}_i(\bar{c})$ . It can be seen that  $\alpha_s$  will induce two possible half angles  $\beta_{s,1}$  and  $\beta_{s,2}$ . By law of cosines,

$$\beta = \frac{\pi}{2} \pm \alpha_s - \arcsin \left( \frac{r_2 - r_1}{2\eta} \right) \quad (109)$$

$$= \frac{\pi}{2} \pm \alpha_s - \arcsin \left( \frac{\sqrt{\eta^2 - n \sin^2 \alpha_s}}{\eta} \right), \quad (110)$$

where  $r_1, r_2$  are the solutions to

$$r^2 - (2\sqrt{n} \cos \alpha_s)r + (n - \eta^2) = 0. \quad (111)$$

The induced half angle  $\beta$  becomes unique once  $\eta > \sqrt{n}$ . This concludes the proof of the approximation. ■

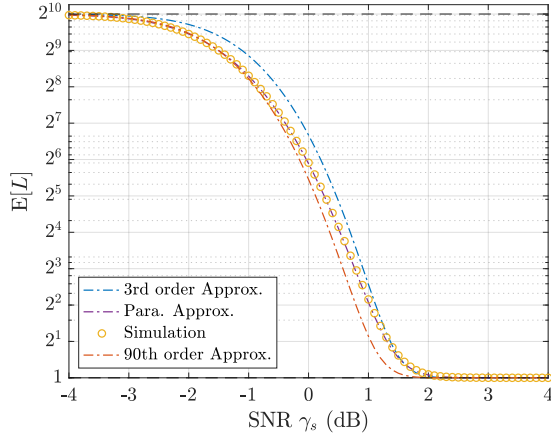


Fig. 10. The expected list rank  $E[L]$  vs. SNR via transformation (97) for ZTCC (561, 753), degree-10 DSO CRC polynomial 0x4CF at  $k = 64$ .

To demonstrate the tightness of the proposed approximation for good enough CRC-CC concatenated codes, Fig. 9 shows the approximations of  $E[L|W = \eta, \mathbf{X} = \bar{\mathbf{x}}_e]$  for ZTCC (561, 753) used with the degree-10 DSO CRC polynomial 0x4CF at  $k = 64$  with  $\mu = 3, 90$ . This concatenated code has a minimum distance  $d_{\min}^l = 20$  and thus can be deemed as good enough. When  $\mu = 3$ , our approximation accurately gives the smaller values of the actual conditional expected list rank. As  $\mu$  increases, the accuracy of the approximation will shift towards large values of conditional expected list rank. Fig. 10 illustrates the approximation of  $E[L]$  vs. SNR via transformation (97). The 3rd-order and 90-th order approximations still behave in the similar fashion as in  $E[L|W = \eta, \mathbf{X} = \bar{\mathbf{x}}_e]$ .

### C. Complexity Analysis

There are a variety of implementations of list decoding of CCs as described in, e.g., [38]–[42]. In this paper, the SLVD implementation maintains a list of path metric differences by using a red-black tree as described in [40], which provides the fastest runtime we found among the data structures that support full floating-point precision. The literature mentioned above also analyzed the number of bit operations or the asymptotic complexity of the algorithms presented, but those complexity metrics are not directly connected with actual runtime. To explore how the additional complexity of SLVD of CRC-ZTCC codes relative to the standard soft Viterbi (SSV) decoding, we develop an average complexity expression that closely approximates our empirical runtimes.

For our specific implementation, three components comprise the average complexity of SLVD, given by

$$C_{\text{SLVD}} = C_{\text{SSV}} + C_{\text{trace}} + C_{\text{list}}. \quad (112)$$

The first component  $C_{\text{SSV}}$  is the complexity required to perform the add-compare-select (ACS) operations on the trellis of the given CC and perform the initial traceback associated

with SSV. Specifically, for CRC-ZTCC codes, this quantity is given by

$$\begin{aligned} C_{\text{SSV}} &= (2^{\nu+1} - 2) + 1.5(2^{\nu+1} - 2) + 1.5(k + m - \nu)2^{\nu+1} \\ &\quad + c_1[2(k + m + \nu) + 1.5(k + m)] \\ &= 5(2^{\nu} - 1) + 3(k + m - \nu)2^{\nu} \\ &\quad + c_1[2(k + m + \nu) + 1.5(k + m)]. \end{aligned} \quad (113)$$

For CRC-TBCC codes, this quantity is given by

$$\begin{aligned} C_{\text{SSV}} &= 1.5(k + m)2^{\nu+1} + 2^{\nu} + 3.5c_1(k + m) \\ &= (3k + 3m + 1)2^{\nu} + 3.5c_1(k + m). \end{aligned} \quad (114)$$

In (113) and (114), we assign 1 unit of complexity to addition per branch and 0.5 units of complexity to compare-select operation per branch. The third term in (113) approximates the complexity of the traceback operation, assigning 2 units of complexity for accessing the parent node per trellis stage and 1.5 units of complexity per codeword symbol for the CRC verification on the decoded sequence  $\hat{\mathbf{v}}$ . For CRC-TBCC codes, it takes  $2^{\nu}$  operations to identify the optimal termination state with minimum metric before the first traceback.

The second component  $C_{\text{trace}}$  represents the complexity of the *additional* traceback operations required by SLVD. Specifically, for a given CRC-ZTCC code,

$$C_{\text{trace}} = c_1(E[L] - 1)[2(k + m + \nu) + 1.5(k + m)]. \quad (115)$$

For CRC-TBCC codes,

$$C_{\text{trace}} = 3.5c_1(E[L] - 1)(k + m). \quad (116)$$

The third component  $C_{\text{list}}$  represents the normalized complexity of inserting new elements to maintain an ordered list of path metric differences. For both CRC-ZTCC codes and CRC-TBCC codes,

$$C_{\text{list}} = c_2 E[I] \log(E[I]), \quad (117)$$

where  $E[I]$  is the expected number of insertions to maintain the sorted list of path metric differences. According to the mechanism of insertion, for CRC-ZTCC codes,

$$E[I] \leq (k + m)E[L], \quad (118)$$

and for CRC-TBCC codes,

$$E[I] \leq (k + m)E[L] + 2^{\nu} - 1, \quad (119)$$

where  $2^{\nu} - 1$  denotes the number of path metric differences between the optimal terminating state and any other  $2^{\nu} - 1$  terminating states.

In (113), (114), (115), (116), and (117) the constants  $c_1$  and  $c_2$  characterizes implementation-specific differences in the implemented complexity of traceback and list insertion (respectively) as compared to the ACS operations of Viterbi decoding. For our implementation, we found  $c_1 = 1.5$  and  $c_2 = 2.2$ .

The additional complexity of the SLVD over SSV decoding is completely characterized by the additional tracebacks along the trellis and the maintenance of an ordered list of path metric differences. We define the *normalized complexity*  $\bar{C}$  as the



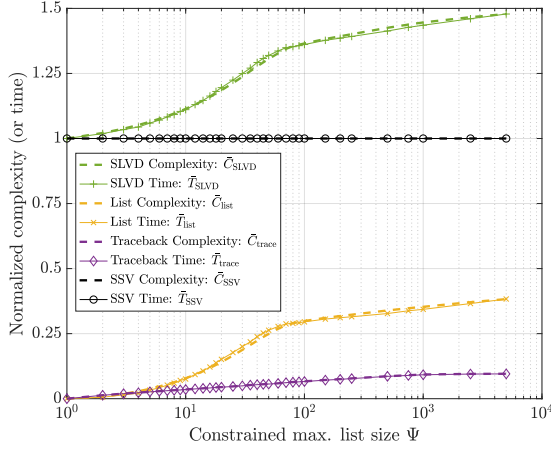


Fig. 11. The complexity of S-LVA with different list sizes for ZTCC (27, 31), and degree-10 DSO CRC poly. 0x709, with  $k = 64$  at SNR  $\gamma_s = 2$  dB. All variables are normalized by the time or complexity of the SSV algorithm. In the simulation setting,  $c_1 = 1.5$  and  $c_2 = 2.2$ .

complexity divided by the complexity required to perform the SSV, i.e.,

$$\bar{C}_{\text{SLVD}} = \frac{C_{\text{SLVD}}}{C_{\text{SSV}}} = 1 + \bar{C}_{\text{trace}} + \bar{C}_{\text{list}}. \quad (120)$$

The normalized complexity provides a measure for the additional complexity of operations associated with the SLVD relative that of the SSV algorithm.

We recorded the runtime  $T_{\text{SLVD}}$ ,  $T_{\text{SSV}}$ ,  $T_{\text{trace}}$ , and  $T_{\text{list}}$  on an Intel i7-4720HQ using Visual C++. We then divided all of these terms by  $T_{\text{SSV}}$  to compute a normalized runtime  $\bar{T}$ . Fig. 11 shows normalized complexity based on equation (120) and normalized runtimes. In both cases, the normalization is computed by dividing by the complexity or run-time associated with SSV, i.e., performing all the add-compare-select (ACS) operations on the trellis and a traceback from the state with the best metric. The normalized complexity and normalized runtime curves are indistinguishable. Fig. 11 also shows that the additional complexity of S-LVA is primarily from maintaining an ordered list of path metric differences.

## V. SIMULATION RESULTS

In this section, we present our simulation results of CRC-ZTCC codes in Table II and CRC-TBCC codes in Table III.

### A. Simulation Results for CRC-ZTCC Codes

Fig. 12 shows the trade-off between the SNR gap to the RCU bound and the average decoding complexity for a target probability of UE  $P_{e,\lambda} = 10^{-4}$ . It is shown that for a given ZTCC, increasing the degree  $m$  of DSO CRC polynomials can significantly diminish the SNR gap to the RCU bound at a relatively small complexity increase. This SNR gap reduction is especially considerable when  $\nu$  is small and becomes less significant as  $\nu$  becomes large. For all ZTCCs, the complexity cost of increasing  $m$  from 3 to 10 is within a factor of 2. This is consistent with Fig. 11 in which the complexity increases by a factor less than 1.5 even for a very large constrained maximum list size  $\Psi$ . The dashed lines in Fig. 12 show how

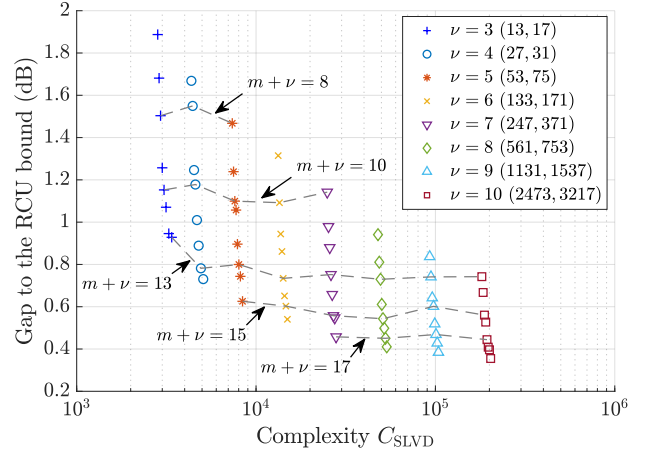


Fig. 12. The SNR gap to the RCU bound vs. the average complexity of SLVD of the family of CRC-ZTCC codes in Table II for target probability of UE  $P_{e,\lambda} = 10^{-4}$ . Each color represents a specific ZTCC shown in parenthesis. Markers from top to bottom with the same color correspond to SSV with no CRC and then DSO CRC polynomials with  $m = 3, 4, \dots, 10$ .

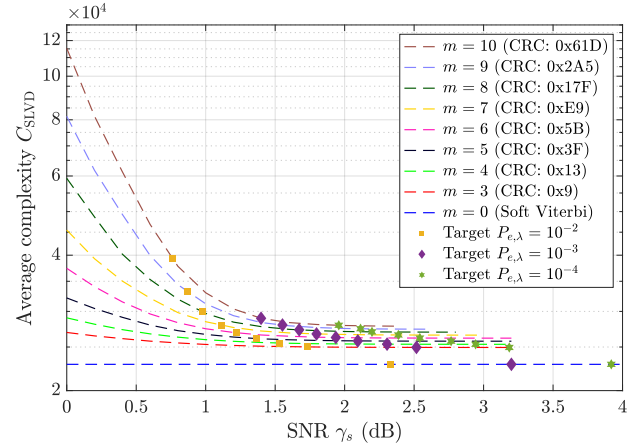


Fig. 13. The average complexity vs. SNR for ZTCC (247, 371) with used with its DSO CRC polynomials. The ZTCC with no CRC using soft Viterbi decoding is also given as a reference.

the RCU gap remains roughly constant for a constant value of  $m + \nu$  which approximates the trellis complexity of the CRC-ZTCC code. However, list decoding with a well chosen  $(m, \nu)$  pair, achieves the performance of this trellis complexity with a minimum implementation complexity  $C_{\text{SLVD}}$ . The termination overhead associated with ZTCC induces a gap from the RCU bound, which can be closed by using the corresponding TBCC as we will see below.

Fig. 13 shows the complexity  $C_{\text{SLVD}}$  computed using (112) as a function of SNR for ZTCC (247, 371) and its DSO CRC polynomials with degree  $m$  from 3 to 10 from Table II. The ZTCC using soft Viterbi decoding with no CRC is also shown. Here, the target probabilities of UE at  $10^{-2}$ ,  $10^{-3}$ ,  $10^{-4}$  for each CRC-ZTCC code are marked by squares, diamonds, and stars, respectively. For each target probability of UE, the corresponding complexity is within a factor of 2 compared to the soft Viterbi decoding of ZTCC (247, 371).

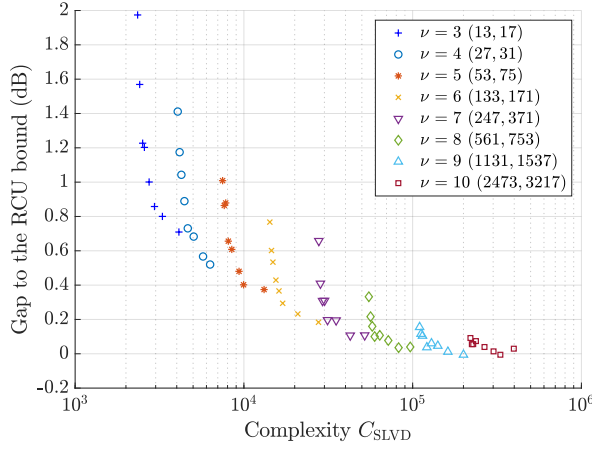


Fig. 14. The SNR gap to the RCU bound vs. the average complexity of SLVD of the family of CRC-TBCC codes in Table III at a target probability of UE  $P_{e,\lambda} = 10^{-4}$ . Each color represents a specific TBCC shown in parenthesis. Markers from top to bottom with the same color correspond to the DSO CRC polynomials with  $m = 3, 4, \dots, 10$ .

### B. Simulation Results for CRC-TBCC Codes

In Sec. II we use the fact that for a CRC-ZTCC code, each SLVD operation yields a valid higher-rate codeword, i.e. a ZTCC codeword. However, for a CRC-TBCC code, SLVD operations do not always yield a valid higher rate codeword, i.e., a TBCC codeword, because the tail-biting condition is often not met. Because of this, we can no longer assume that  $\bar{L} \approx 2^m$ . Nevertheless, Approximations 3 and 4 still apply for an accurate estimation of  $\bar{L}$ , obtained for example by simulation.

The increased value of  $\bar{L}$  may be understood by considering the higher-rate code  $C_h$  to be the pseudo code represented by all paths on the trellis regardless of whether they meet the TB condition. Due to the additional complexity required to check the TB condition,  $E[I]$  is significantly increased compared to the CRC-ZTCC code. While we identified the empirical value of  $E[I]$  for CRC-ZTCC codes, in this section we simply assume  $E[I] = (k + m)E[L] + 2^\nu - 1$  for CRC-TBCC codes. Hence, using (114), (116) with  $c_1 = 1$ , (117) with  $c_2 = 1$ , together with the aforementioned assumption on  $E[I]$ , we can compute an estimate of the average complexity  $C_{\text{SLVD}}$  of our implementation of SLVD of CRC-TBCC codes.

Fig. 14 shows the SNR gap to the RCU bound vs. the average complexity for target probability of UE  $P_{e,\lambda} = 10^{-4}$  for all CRC-TBCC codes designed in Table III. Compared to Fig. 12, TB encoding significantly reduces the SNR gap to the RCU, because the overhead of termination is avoided. However, this reduction of the gap comes at the expense of a slight increase in average complexity for checking the TB conditions. Note the exciting result that some CRC-TBCC codes outperform the RCU bound for  $\nu = 9$  and 10. Another phenomenon distinct from CRC-ZTCC codes is that for TBCCs with large  $\nu$ , increasing the CRC polynomial degree from  $m = 3$  to  $m = 10$  does not provide a visible benefit. Note, however, that the  $m = 3$  CRC does provide a benefit over a TBCC used with no CRC.

To illustrate the performance of the best CRC-TBCC codes

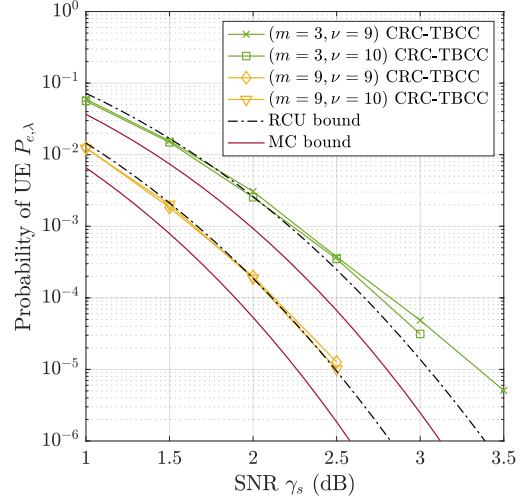


Fig. 15. Comparison between  $P_{e,\lambda}$  and RCU and MC bounds at rate  $R = 64/134$  (i.e.,  $m = 3$ ) and  $R = 64/146$  (i.e.,  $m = 9$ ) for the CRC-TBCC codes designed in Table III. For the best of clarity, only  $\nu = 9, 10$  TBCCs are displayed.

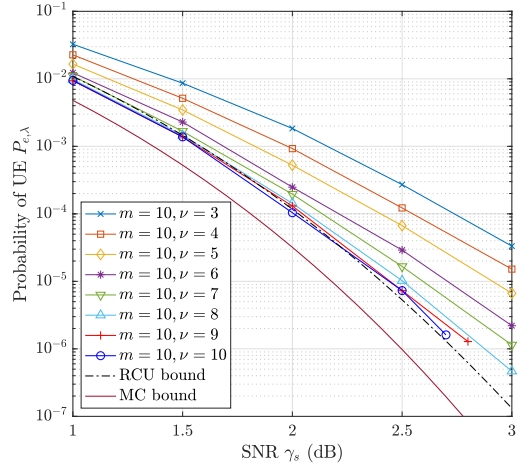


Fig. 16. Comparison between  $P_{e,\lambda}$  and RCU and MC bounds at rate  $R = 64/148$  (i.e.,  $m = 10$ ) for the CRC-TBCC codes designed in Table III.

designed in Table III, we select  $\nu = 9$  and  $\nu = 10$  TBCCs as an example. Fig. 15 shows two cases of rate  $R = 64/134$  corresponding to  $m = 3$  and  $R = 64/146$  corresponding to  $m = 9$ . The MC bound and the RCU bounds for these rates are plotted using the saddlepoint approximations provided in Approximations 1 and 2, respectively. We see that in these two cases, the CRC-TBCC codes in Fig. 15 beat the RCU bound at low SNR values. However, this superiority gradually fades away as SNR increases, although for  $m = 9$ , the performance is very close to the RCU bound even at probability of UE  $10^{-5}$ . Simulations also suggest that it is extremely difficult to further improve the code performance once beyond the RCU bound at low probability of UE.

Fig. 16 shows the family of CRC-TBCC codes with  $k = 64$  and  $n = 148$  (corresponding to  $m = 10$ ). For small  $\nu$  is small, we see a visible improvement as  $\nu$  increases. However, once performance reaches the RCU bound, further increase in  $\nu$  provides little benefit. For example with  $m = 10$ , the CRC-

TBCC code with  $\nu = 9$  attains similar performance of that with  $\nu = 10$ .

## VI. CONCLUSION

In this paper, we consider CRC-CC concatenated codes as a promising good short blocklength codes. The concatenated nature permits the use of SLVD that allows the code to attain the ML decoding performance at low complexity. We identified the DSO CRC polynomial for a family of most popular ZTCCs and TBCCs at sufficiently low target probability of UE. Because of the overhead required for termination, no CRC-ZTCC codes were able to outperform the RCU bound. This situation is ameliorated when TB encoding is considered. Several CRC-TBCC codes beat the RCU bound at practically interesting values of probability of UE.

Direct comparisons with other codes requires the added complexity of puncturing to match rates. Unfortunately, we have excluded puncturing from this paper for simplicity. Nevertheless, for explicit comparisons of other short blocklength codes to punctured CRC-TBCC codes with exactly the same rate, we direct the reader to [2] which shows that punctured CRC-TBCC codes outperform all the codes surveyed in [7] except for  $\nu = 14$  under WAVA, which requires an extremely complex decoder.

To show the excellent performance of the CRC-CC paradigm in an absolute sense, this paper provides results with respect to the RCU bound. In this way, the gap to RCU bound can be easily compared with both previous and future short-blocklength designs with similar rates and blocklengths. Fig. 12 shows that the CRC-ZTCC code with  $\nu = 8$  and  $m = 10$  performs within 0.4 dB of the RCU bound for probability of UE  $10^{-4}$ . Fig. 14 shows that the CRC-TBCC code with  $\nu = 8$  and  $m = 9$  essentially attains the RCU bound for probability of UE  $10^{-4}$ . Thus, this CRC-TBCC code achieves a similar proximity to the RCU bound as the  $\nu = 14$  TBCC under WAVA from [2], [7], but with less decoder complexity than a TBCC with  $\nu = 9$  as shown in Fig. 14.

The beauty of SLVD lies in the fact that its average complexity is governed by its expected list rank  $E[L]$ , a quantity that is inversely proportional to the SNR value. This allows a huge complexity reduction at interesting operating SNR values that guarantee a low target probability of UE. In particular, the parametric approximation of  $E[L]$  provides an explicit characterization of the performance-complexity tradeoff. It shows that for CRC-ZTCC codes with a target error probability  $P_{e,\lambda}^*$  and  $\bar{L} \approx 2^m$ , a CRC degree  $m \leq -\log(P_{e,\lambda}^*)$  is sufficient to maintain  $E[L] \leq 2$ . For a good CRC-ZTCC code with CRC degree  $m$ , the behavior of  $E[L]$  can be well approximated using the proposed onion model. However, the behavior of the supremum list rank  $\lambda$  is less understood and is worth future investigation.

## APPENDIX A

### DERIVATION OF THE INDUCED DENSITY FUNCTION

Let  $\mathcal{B}(a, r)$  denote the spherical surface of center  $a$  and radius  $r$  in  $\mathbb{R}^n$ . In this section, we derive the induced density function  $g_w(\mathbf{y}_p)$  incurred when projecting a received point  $\mathbf{y}$

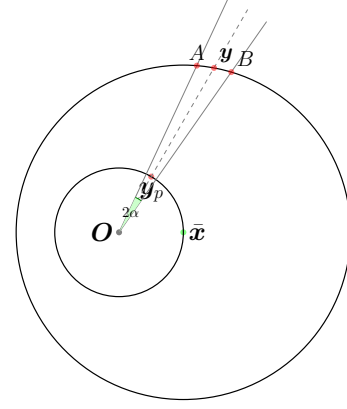


Fig. 17. Derivation of the induced density function  $g_w(\mathbf{y}_p)$  in  $\mathbb{R}^n$ .

uniformly distributed on  $\mathcal{B}(\bar{\mathbf{x}}, w)$  to point  $\mathbf{y}_p = (r/\|\mathbf{y}\|)\mathbf{y}$  that lies on the codeword sphere  $\mathcal{B}(\mathbf{O}, A\sqrt{n})$  in  $\mathbb{R}^n$ . Fig. 17 depicts this scenario in  $\mathbb{R}^n$ . For our purposes, we assume that  $w \geq A\sqrt{n}$  to ensure the bijective relationship between  $\mathbf{y}$  and  $\mathbf{y}_p$ .

Let us consider a circular cone  $Q_\alpha$  in  $\mathbb{R}^n$  with apex at the origin  $\mathbf{O}$ , axis along  $\mathbf{O}\mathbf{y}_p$  and half angle  $\alpha$ . Algebraically, define the direction vectors

$$\mathbf{y}_e \triangleq \frac{\mathbf{y}}{\|\mathbf{y}\|} \quad (121)$$

$$\mathbf{z}_e \triangleq \frac{\mathbf{y} - \bar{\mathbf{x}}}{\|\mathbf{y} - \bar{\mathbf{x}}\|}. \quad (122)$$

Hence, the circular cone  $Q_\alpha$  is given by

$$\begin{aligned} Q_\alpha &= \left\{ \mathbf{r} \in \mathbb{R}^n : \frac{\mathbf{r}^\top \mathbf{y}_e}{\|\mathbf{r}\|} \geq \cos \alpha \right\} \\ &= \left\{ \mathbf{r} \in \mathbb{R}^n : (\mathbf{r} - \mathbf{O})^\top (I - \epsilon^2(\alpha) \mathbf{y}_e \mathbf{y}_e^\top) (\mathbf{r} - \mathbf{O}) \leq 0 \right\}, \end{aligned} \quad (123)$$

where  $\epsilon(\alpha) \triangleq 1/\cos \alpha$  denotes the eccentricity of the cone. Cone  $Q_\alpha$  intersects with the noise sphere  $\mathcal{B}(\bar{\mathbf{x}}, w)$ , thus producing a surface area  $Q_\alpha \cap \mathcal{B}(\bar{\mathbf{x}}, w)$  delimited by  $A, B$  on Fig. 17. Thus, the induced density at  $\mathbf{y}_p$  is given by

$$g_w(\mathbf{y}_p) = \lim_{\alpha \rightarrow 0} \frac{S(Q_\alpha \cap \mathcal{B}(\bar{\mathbf{x}}, w))/S_{n-1}(w)}{S(Q_\alpha \cap \mathcal{B}(\mathbf{O}, A\sqrt{n}))}, \quad (124)$$

where  $S(\cdot)$  denotes the surface area in  $\mathbb{R}^n$ . Note that for sufficiently small  $\alpha$ , the spherical surface around  $\mathbf{y}$  is equivalent to the tangent hyperplane at  $\mathbf{y}$ , given by

$$\begin{aligned} H &= \left\{ \mathbf{r} \in \mathbb{R}^n : \mathbf{z}_e^\top (\mathbf{r} - \mathbf{y}) = 0 \right\} \\ &= \left\{ \mathbf{r} \in \mathbb{R}^n : \mathbf{z}_e^\top (\mathbf{r} - \mathbf{O}) = \hat{h} \right\}, \end{aligned} \quad (125)$$

where  $\hat{h} \triangleq \mathbf{z}_e^\top \mathbf{y}$ . Define  $\rho \triangleq \sqrt{1 - (\mathbf{z}_e^\top \mathbf{y}_e)^2}$ . Thus, using the result by Dearing [43, Eq. (15)], if  $\epsilon(\alpha)\rho < 1$ , the intersection of hyperplane  $H$  and cone  $Q_\alpha$  is an ellipsoid of dimension  $(n - 1)$ , which, after proper rotation  $T$  around  $\mathbf{O}$ , can be written as

$$\begin{aligned} &T(Q_\alpha) \cap T(H) \\ &= \left\{ (r_1, \dots, r_{n-1}, \hat{h}) : \frac{(r_1 - \hat{c}_1)^2}{\hat{a}^2} + \frac{\sum_{j=2}^{n-1} (r_j - \hat{c}_j)^2}{\hat{b}} = 1 \right\}, \end{aligned}$$

where

$$\sigma = \mathbf{z}_e^\top \mathbf{y}_e \quad (126)$$

$$\hat{c}_1 = \frac{\epsilon^2(\alpha)\rho\sigma\hat{h}}{1 - \epsilon^2(\alpha)\rho^2}, \quad \hat{c}_j = 0, \quad j = 2, \dots, n-1 \quad (127)$$

$$\hat{a}^2 = \frac{(\epsilon^2(\alpha) - 1)\hat{h}^2}{(1 - \epsilon^2(\alpha)\rho^2)^2} \quad (128)$$

$$\tilde{b} = \hat{a}^2(1 - \epsilon^2(\alpha)\rho^2). \quad (129)$$

Since  $\mathbf{z}_e$  and  $\mathbf{y}_e$  are non-orthogonal,  $1/\rho > 1$ . Hence, for sufficiently small  $\alpha$ ,  $\epsilon(\alpha) < 1/\rho$  and thus Dearing's result follows. Summarizing the analysis above, we obtain

$$\lim_{\alpha \rightarrow 0} S(Q_\alpha \cap \mathcal{B}(\bar{\mathbf{x}}, w)) \quad (130)$$

$$= \lim_{\alpha \rightarrow 0} S(T(Q_\alpha) \cap T(H)) \quad (131)$$

$$= \lim_{\alpha \rightarrow 0} \frac{\pi^{\frac{n-1}{2}}}{\Gamma(\frac{n+1}{2})} \hat{a}(\sqrt{\tilde{b}})^{n-2} \quad (132)$$

$$= \lim_{\alpha \rightarrow 0} \frac{\pi^{\frac{n-1}{2}}}{\Gamma(\frac{n+1}{2})} \left( \frac{(\epsilon^2(\alpha) - 1)\hat{h}^2}{(1 - \epsilon^2(\alpha)\rho^2)^2} \right)^{\frac{n-1}{2}} (1 - \epsilon^2(\alpha)\rho^2)^{\frac{n-2}{2}} \quad (133)$$

$$= \lim_{\alpha \rightarrow 0} \frac{\pi^{\frac{n-1}{2}}}{\Gamma(\frac{n+1}{2})} 2^{\frac{n-1}{2}} (\epsilon(\alpha) - 1)^{\frac{n-1}{2}} \hat{h}^{n-1} (\mathbf{z}_e^\top \mathbf{y}_e)^{-n} \quad (134)$$

$$= \lim_{\alpha \rightarrow 0} \frac{\pi^{\frac{n-1}{2}}}{\Gamma(\frac{n+1}{2})} 2^{\frac{n-1}{2}} \left( \frac{1 - \cos \alpha}{\cos \alpha} \right)^{\frac{n-1}{2}} \left( \frac{\mathbf{z}_e^\top \mathbf{y}}{\mathbf{z}_e^\top \mathbf{y}_e} \right)^{n-1} \frac{1}{\mathbf{z}_e^\top \mathbf{y}_e} \quad (135)$$

$$= \lim_{\alpha \rightarrow 0} \frac{\pi^{\frac{n-1}{2}}}{\Gamma(\frac{n+1}{2})} 2^{\frac{n-1}{2}} \left( 2 \sin^2 \left( \frac{\alpha}{2} \right) \right)^{\frac{n-1}{2}} \frac{\|\mathbf{y}\|^{n-1}}{\cos \angle \bar{\mathbf{x}} \mathbf{y} \mathbf{O}} \quad (136)$$

$$= \lim_{\alpha \rightarrow 0} \frac{\pi^{\frac{n-1}{2}}}{\Gamma(\frac{n+1}{2})} \alpha^{n-1} \frac{\|\mathbf{y}\|^{n-1}}{\cos \angle \bar{\mathbf{x}} \mathbf{y} \mathbf{O}}, \quad (137)$$

where (130) to (131) follows since for sufficiently small half angle, the spherical surface around  $\mathbf{y}$  is equivalent to that of the tangent hyperplane  $H$  at  $\mathbf{y}$ . From Shannon [18, Eq. (21)],

$$\begin{aligned} S(Q_\alpha \cap \mathcal{B}(\mathbf{O}, A\sqrt{n})) \\ = \frac{(n-1)\pi^{\frac{n-1}{2}}(A\sqrt{n})^{n-1}}{\Gamma(\frac{n+1}{2})} \int_0^\alpha \sin^{n-2} \theta d\theta. \end{aligned} \quad (138)$$

Substituting (137), (138) into (124), we obtain

$$\begin{aligned} g_w(\mathbf{y}_p) &= \lim_{\alpha \rightarrow 0} \frac{S(Q_\alpha \cap \mathcal{B}(\bar{\mathbf{x}}, w))}{S(Q_\alpha \cap \mathcal{B}(\mathbf{O}, A\sqrt{n}))} \frac{S_{n-1}(A\sqrt{n})}{S_{n-1}(w)} \frac{1}{S_{n-1}(A\sqrt{n})} \\ &= \lim_{\alpha \rightarrow 0} \frac{\alpha^{n-1} \frac{\|\mathbf{y}(\mathbf{y}_p)\|^{n-1}}{\cos \angle \bar{\mathbf{x}} \mathbf{y} \mathbf{O}}}{(n-1) \int_0^\alpha \theta^{n-2} d\theta} \frac{1}{w^{n-1}} \frac{1}{S_{n-1}(A\sqrt{n})} \\ &= \left( \frac{\|\mathbf{y}(\mathbf{y}_p)\|}{w} \right)^{n-1} \frac{1}{\cos \angle \bar{\mathbf{x}} \mathbf{y} \mathbf{O}} \frac{1}{S_{n-1}(A\sqrt{n})}, \end{aligned} \quad (139)$$

where  $\mathbf{y}(\mathbf{y}_p)$  is the pre-image of  $\mathbf{y}_p$  on the noise sphere  $\mathcal{B}(\bar{\mathbf{x}}, w)$ . Here, (139) is the induced density function of  $\mathbf{y}_p \in \mathcal{B}(\mathbf{O}, A\sqrt{n})$ . Observe that it is rotationally symmetric with respect to axis  $\mathbf{O}\bar{\mathbf{x}}$ .

Next, we give an alternative expression of  $g_w(\mathbf{y}_p)$  to derive its upper bound and lower bound. First, we rotate the coordinate system such that axis  $\mathbf{O}\bar{\mathbf{x}}$  is the first coordinate and the

rest of  $(n-1)$  coordinates are orthogonal to  $\mathbf{O}\bar{\mathbf{x}}$ . In the new coordinate system, let  $\bar{\mathbf{x}} = (A\sqrt{n}, 0, \dots, 0) \in \mathbb{R}^n$ . Hence, for an arbitrary projected point  $\mathbf{y}_p = (y_1, y_2, \dots, y_n) \in \mathcal{B}(\mathbf{O}, A\sqrt{n})$ , assume that  $\rho \triangleq \|\mathbf{y}(\mathbf{y}_p)\|$ . Thus,

$$\mathbf{y}(\mathbf{y}_p) = \frac{\rho}{A\sqrt{n}}(y_1, y_2, \dots, y_n). \quad (140)$$

Since  $\mathbf{y}(\mathbf{y}_p) \in \mathcal{B}(\bar{\mathbf{x}}, w)$ ,

$$\left( \frac{\rho}{A\sqrt{n}} y_1 - A\sqrt{n} \right)^2 + \left( \frac{\rho}{A\sqrt{n}} \right)^2 \sum_{i=2}^n y_i^2 = w^2. \quad (141)$$

Solving for  $\rho$  yields

$$\rho = y_1 + \sqrt{y_1^2 + w^2 - A^2 n}. \quad (142)$$

By law of cosines, it is shown that

$$\cos \angle \bar{\mathbf{x}} \mathbf{y} \mathbf{O} = \frac{\rho^2 + w^2 - A^2 n}{2\rho w} = \frac{\sqrt{y_1^2 + w^2 - A^2 n}}{w}. \quad (143)$$

Hence, substituting (142) and (143) into (139) and expressing  $g_w(\mathbf{y}_p)$  in terms of  $y_1 \in [-A\sqrt{n}, A\sqrt{n}]$ , we obtain

$$\begin{aligned} g_w(y_1) &= \frac{1}{S_{n-1}(A\sqrt{n})} \frac{(y_1 + \sqrt{y_1^2 + w^2 - A^2 n})^{n-2}}{w^{n-2}} \\ &\quad \cdot \left( 1 + \frac{y_1}{\sqrt{y_1^2 + w^2 - A^2 n}} \right). \end{aligned} \quad (144)$$

Clearly,  $g_w(y_1)$  is monotonically increasing in  $y_1$ . Hence,

$$g_w(y_1) \geq g_w(-A\sqrt{n}) = \frac{1}{S_{n-1}(A\sqrt{n})} \left( 1 - \frac{A\sqrt{n}}{w} \right)^{n-1} \quad (145)$$

$$g_w(y_1) \leq g_w(A\sqrt{n}) = \frac{1}{S_{n-1}(A\sqrt{n})} \left( 1 + \frac{A\sqrt{n}}{w} \right)^{n-1}. \quad (146)$$

Geometrically, this implies that the maximum induced density is attained at the transmitted point  $\bar{\mathbf{x}}$  whereas the minimum induced density is attained at  $-\bar{\mathbf{x}}$ .

## REFERENCES

- [1] H. Yang, S. V. S. Ranganathan, and R. D. Wesel, "Serial list Viterbi decoding with CRC: Managing errors, erasures, and complexity," in *2018 IEEE Global Commun. Conf. (GLOBECOM)*, Dec 2018, pp. 1–6.
- [2] E. Liang, H. Yang, D. Divsalar, and R. D. Wesel, "List-decoded tail-biting convolutional codes with distance-spectrum optimal CRCs for 5G," in *2019 IEEE Global Commun. Conf. (GLOBECOM)*, 2019, pp. 1–6.
- [3] H. Yang, L. Wang, V. Lau, and R. D. Wesel, "An efficient algorithm for designing optimal CRCs for tail-biting convolutional codes," in *Proc. 2020 IEEE Int. Symp. Inf. Theory (ISIT)*, 2020, pp. 292–297.
- [4] H. Ji, S. Park, J. Yeo, Y. Kim, J. Lee, and B. Shim, "Ultra-reliable and low-latency communications in 5G downlink: Physical layer aspects," *IEEE Wireless Commun. Mag.*, vol. 25, no. 3, pp. 124–130, 2018.
- [5] Y. Polyanskiy, H. V. Poor, and S. Verdú, "Channel coding rate in the finite blocklength regime," *IEEE Trans. Inf. Theory*, vol. 56, no. 5, pp. 2307–2359, May 2010.
- [6] J. Font-Segura, G. Vazquez-Vilar, A. Martinez, A. Guillén i Fàbregas, and A. Lancho, "Saddlepoint approximations of lower and upper bounds to the error probability in channel coding," in *2018 52nd Annual Conf. Inf. Sci. Syst. (CISS)*, 2018, pp. 1–6.
- [7] M. C. Coşkun, G. Durisi, T. Jerkovits, G. Liva, W. Ryan, B. Stein, and F. Steiner, "Efficient error-correcting codes in the short blocklength regime," *Physical Commun.*, vol. 34, pp. 66 – 79, 2019.

- [8] M. P. C. Fossorier and Shu Lin, "Soft-decision decoding of linear block codes based on ordered statistics," *IEEE Trans. Inf. Theory*, vol. 41, no. 5, pp. 1379–1396, 1995.
- [9] C. Yue, M. Shirvanimoghaddam, B. Vucetic, and Y. Li, "A revisit to ordered statistics decoding: Distance distribution and decoding rules." [Online]. Available: <http://arxiv.org/abs/2004.04913>
- [10] L. Gaudio, T. Ninnacs, T. Jerkovits, and G. Liva, "On the performance of short tail-biting convolutional codes for ultra-reliable communications," in *SCC 2017; 11th Int. ITG Conf. Syst., Commun., and Coding*, Feb 2017, pp. 1–6.
- [11] L. Dolecek, D. Divsalar, Y. Sun, and B. Amiri, "Non-binary protograph-based LDPC codes: Enumerators, analysis, and designs," *IEEE Trans. Inf. Theory*, vol. 60, no. 7, pp. 3913–3941, 2014.
- [12] S. V. S. Ranganathan, D. Divsalar, and R. D. Wesel, "Quasi-cyclic protograph-based raptor-like LDPC codes for short block-lengths," *IEEE Trans. Inf. Theory*, vol. 65, no. 6, pp. 3758–3777, 2019.
- [13] T. Jerkovits and B. Matuz, "Turbo code design for short blocks," in *2016 8th Advanced Satellite Multimedia Syst. Conf. and the 14th Signal Processing for Space Commun. Workshop (ASMS/SPSC)*, 2016, pp. 1–6.
- [14] E. Arkan, "Channel polarization: A method for constructing capacity-achieving codes for symmetric binary-input memoryless channels," *IEEE Trans. Inf. Theory*, vol. 55, no. 7, pp. 3051–3073, 2009.
- [15] I. Tal and A. Vardy, "List decoding of polar codes," *IEEE Trans. Inf. Theory*, vol. 61, no. 5, pp. 2213–2226, 2015.
- [16] E. Arkan, "From sequential decoding to channel polarization and back again." [Online]. Available: <http://arxiv.org/abs/1908.09594>
- [17] H. Yao, A. Fazeli, and A. Vardy, "List decoding of Arkan's PAC codes," in *2020 IEEE Int. Symp. Inf. Theory (ISIT)*, 2020, pp. 443–448.
- [18] C. E. Shannon, "Probability of error for optimal codes in a Gaussian channel," *Bell Syst. Tech. J.*, vol. 38, no. 3, pp. 611–656, May 1959.
- [19] P. Elias, "Coding for noisy channels," *Proc. IRE. Conv. Rec. pt. 4*, vol. 3, pp. 37 – 46, 1955.
- [20] A. Viterbi, "Error bounds for convolutional codes and an asymptotically optimum decoding algorithm," *IEEE Trans. Inf. Theory*, vol. 13, no. 2, pp. 260–269, 1967.
- [21] G. D. Forney, "The Viterbi algorithm," *Proc. IEEE*, vol. 61, no. 3, pp. 268–278, 1973.
- [22] —, "Convolutional codes II. maximum-likelihood decoding," *Inf. Contr.*, vol. 25, no. 3, pp. 222–266, 1974.
- [23] W. W. Peterson and D. T. Brown, "Cyclic codes for error detection," *Proc. IRE*, vol. 49, no. 1, pp. 228–235, 1961.
- [24] M. Rice, "Comparative analysis of two realizations for hybrid-ARQ error control," in *1994 IEEE Global Commun. Conf. (GLOBECOM)*, 1994, pp. 115–119.
- [25] "3GPP TS 25.212 version 7.0.0 release 7," European Telecommunications Standards Institute, Tech. Rep., 2006.
- [26] N. Seshadri and C. W. Sundberg, "List Viterbi decoding algorithms with applications," *IEEE Trans. Commun.*, vol. 42, no. 234, pp. 313–323, Feb 1994.
- [27] H. Ma and J. Wolf, "On tail biting convolutional codes," *IEEE Trans. Commun.*, vol. 34, no. 2, pp. 104–111, February 1986.
- [28] C. Lou, B. Daneshrad, and R. D. Wesel, "Convolutional-code-specific CRC code design," *IEEE Trans. Commun.*, vol. 63, no. 10, pp. 3459–3470, 2015.
- [29] Q. Wang and V. K. Bhargava, "An efficient maximum likelihood decoding algorithm for generalized tail biting convolutional codes including quasicyclic codes," *IEEE Trans. Commun.*, vol. 37, no. 8, pp. 875–879, Aug 1989.
- [30] R. V. Cox and C. E. W. Sundberg, "An efficient adaptive circular Viterbi algorithm for decoding generalized tailbiting convolutional codes," *IEEE Trans. Veh. Technol.*, vol. 43, no. 1, pp. 57–68, Feb 1994.
- [31] J. B. Anderson and S. M. Hladik, "Tailbiting MAP decoders," *IEEE J. Sel. Areas Commun.*, vol. 16, no. 2, pp. 297–302, Feb 1998.
- [32] R. Y. Shao, Shu Lin, and M. P. C. Fossorier, "Two decoding algorithms for tailbiting codes," *IEEE Trans. Commun.*, vol. 51, no. 10, pp. 1658–1665, Oct 2003.
- [33] P. Shankar, P. N. A. Kumar, K. Sasidharan, B. S. Rajan, and A. S. Madhu, "Efficient convergent maximum likelihood decoding on tail-biting trellises." [Online]. Available: <https://arxiv.org/abs/cs/0601023>
- [34] R. Koetter and A. Vardy, "The structure of tail-biting trellises: minimality and basic principles," *IEEE Trans. Inf. Theory*, vol. 49, no. 9, pp. 2081–2105, Sep. 2003.
- [35] T. M. Cover and J. A. Thomas, *Elements of Information Theory*, 2nd ed. New Jersey, USA: Wiley, 2006.
- [36] H. Yang, "Github repository: CRC design for ZTCCs." [Online]. Available: [https://github.com/hengjie-yang/DSO\\_CRC\\_Design\\_for\\_ZTCCs](https://github.com/hengjie-yang/DSO_CRC_Design_for_ZTCCs)
- [37] —, "Github repository: CRC design for TBCCs." [Online]. Available: [https://github.com/hengjie-yang/DSO\\_CRC\\_Design\\_for\\_TBCCs](https://github.com/hengjie-yang/DSO_CRC_Design_for_TBCCs)
- [38] Chunlong Bai, B. Mielczarek, W. A. Krzymien, and I. J. Fair, "Efficient list decoding for parallel concatenated convolutional codes," in *2004 IEEE 15th Int. Symp. Personal, Indoor and Mobile Radio Commun.*, vol. 4, 2004, pp. 2586–2590.
- [39] L. Lijofi, D. Cooper, and B. Canpolat, "A reduced complexity list single-wrong-turn (SWT) Viterbi decoding algorithm," in *2004 IEEE 15th Int. Symp. Personal, Indoor and Mobile Radio Commun.*, vol. 1, 2004, pp. 274–279.
- [40] M. Roder and R. Hamzaoui, "Fast tree-trellis list Viterbi decoding," *IEEE Trans. Commun.*, vol. 54, no. 3, pp. 453–461, Mar. 2006.
- [41] J. Kim, J. Tak, H. Kwak, and J. No, "A new list decoding algorithm for short-length TBCCs with CRC," *IEEE Access*, vol. 6, pp. 35 105–35 111, 2018.
- [42] M. Shirvanimoghaddam, M. S. Mohammadi, R. Abbas, A. Minja, C. Yue, B. Matuz, G. Han, Z. Lin, W. Liu, Y. Li, S. Johnson, and B. Vucetic, "Short block-length codes for ultra-reliable low latency communications," *IEEE Commun. Mag.*, vol. 57, no. 2, pp. 130–137, 2019.
- [43] P. M. Dearing, "Intersections of hyperplanes and conic sections in  $\mathbb{R}^n$ ." [Online]. Available: <http://arxiv.org/abs/1702.03205>